Microporous and Mesoporous Materials 415 (2026) 114368

Contents lists available at ScienceDirect

Microporous and Mesoporous Materials

journal homepage: www.elsevier.com/locate/micromeso

Beyond the size: Assessing the influence of synthesis parameters on ZIF-8 monolith degradation in aqueous environments

Jose de Jesus Velazquez-Garcia [a,*], Susann Frenzke [a], Dina Huanaco-Quispe [b], Henry Sanchez Cornejo [c,d], Luis de los Santos Valladares [c,d], Crispin H.W. Barnes [c], Christopher Copeman [e], Jatinder Singh [e], Stefanie Haugg [f], Dirk Eifler [g], Simone Techert [a,h]

[a] Deutsches Elektronen-Synchrotron DESY, Notkestr. 85, Hamburg, 22607, Germany
[b] Escuela Académica de Ingeniería y Gestión Ambiental, Universidad Nacional Autónoma de Huanta, Jr. Manco Capac 497, Huanta, Ayacucho, Peru
[c] Cavendish Laboratory, Department of Physics, University of Cambridge, Cambridge, CB3 0HE, United Kingdom
[d] Laboratorio de Ceramicos y Nanomateriales, Facultad de Ciencias Fisicas, Universidad Nacional Mayor de San Marcos, Lima, 14-0149, Peru
[e] Department of Chemistry and Biochemistry, Concordia University, 7141 Sherbrooke St W., Montréal, QC, Canada
[f] Center for Hybrid Nanostructures, Universität Hamburg, Luruper Chaussee 149, Hamburg, 22761, Germany
[g] Department of Chemistry, University of Hamburg, Martin-Luther-King-Platz 6, Hamburg, 20146, Germany
[h] Institut für Röntgenphysik, Georg-August-Universität Göttingen, Friedrich-Hund-Platz 1, Göttingen, 37077, Germany

A B S T R A C T

This article reports the room-temperature synthesis of ZIF-8 monoliths, systematically varying synthesis parameters while maintaining a constant metal:ligand ratio of 1:7.9. The washing procedure, aging time, centrifugal speed, precursor concentration, solvent type, ammonia concentration, and metal salt were changed to investigate their effect on the water stability of the resulting monolith. The synthesised monoliths were characterised by optical microscopy, powder X-ray diffraction (PXRD), thermogravimetric analysis (TGA) and N_2 gas adsorption, while the precursor nanocrystallites were analysed by scanning electron microscopy (SEM). Water stability was evaluated by immersing monolithic pieces in Mili-Q water for 24 h, followed by UV-Vis spectroscopy to track linker release and inductive coupled plasma optical emission spectroscopy (ICP-OES) to quantify metal ion leaching. The use of $Zn(CH_3COO)_2$, along with the washing procedure, are the most important parameters for improving water stability and enhancing the phase purity, textural properties and transparency of the monolith. Other parameters contributing to these characteristics are centrifugal speeds exceeding 4200 rpm, concentrated synthesis, and partial replacement of methanol for aqueous ammonia. Based on this comprehensive analysis, a refined synthesis protocol was formed, yielding a more water-stable ZIF-8 monolith. However, despite its improved stability, the monolith was unable to adsorb rhodamine B from aqueous solutions as the dye's size far exceeds the pore window of ZIF-8, limiting adsorption to the external surface.

1. Introduction

Zeolitic imidazolate frameworks (ZIFs) represent new materials falling into the large group known as metal-organic frameworks (MOFs) [1,2]. Among the reported ZIFs, ZIF-8 is one of the most widely used due its simple synthesis coupled with its high thermal and chemical stability [3,4]. Additionally, its structural pore uniformity and high surface area makes ZIF-8 a promising candidate for a wide number of applications, such as gas adsorption, material storage, catalysis, supercapacitors and drug delivery [2,4–9].

Each application requires tailored material properties, which can be achieved by selecting the appropriate synthesis method and optimising its parameters. Therefore, various synthesis approaches have been used to synthesise ZIF-8, including solvothermal, sonochemical, and microfluidic synthesis [9–11]. Regardless of the synthesis method, key reaction parameters, such as solvent composition, temperature, metal: linker ratio, precursor concentration and pH, play a key role in controlling the properties of the final material [12]. Thus, various publications in literature have reported the influence of synthesis parameters in the properties of ZIF-8. For example, Sanchez Cereceda et al. found that increasing the concentration of 2-methylimidazole linker (2mIm) led to larger particle sizes, while solvent and temperature play a critial role in determining porosity [13]. Zhang et al. determined that 8 was the optimum Zn^{2+}:2mIm ratio to obtain the largest surface area [14]. Bustamante et al. reported an ultra-fast crystallisation (60 s) in alcoholic solvents, compared to other solvents, and when methanol was used, a larger particle size was obtained using lower amount of the solvent [15]. Finally, Sheng et al. considered that the water stability of ZIF-8 was improved by using zinc acetate as initial reagent instead of zinc nitrate or zinc chloride [16].

* Corresponding author.
E-mail address: jose.velazquez@desy.de (J.J. Velazquez-Garcia).

https://doi.org/10.1016/j.micromeso.2026.114368
Received 28 June 2026; Received in revised form 10 August 2026; Accepted 15 August 2026
Available online 28 August 2026

Table 1
Synthesis parameters for ZIF-8 monoliths.[a]

Name	Washing	Aging time (h)	Centrifuge rotational speed (rpm)	R-OH	$V_{R\text{-}OH}$ (mL)	$V_{NH3(aq)}$ (mL)	Metal salt
ZIF-8^{mono}	No	1	4200	MeOH	400	0	$Zn(NO_3)_2$
ZIF-8^{mono}-w	Yes	1	4200	MeOH	400	0	$Zn(NO_3)_2$
ZIF-8^{mono}-24 h	No	24	4200	MeOH	400	0	$Zn(NO_3)_2$
ZIF-8^{mono}-48 h	No	48	4200	MeOH	400	0	$Zn(NO_3)_2$
ZIF-8^{mono}-2000 rpm	No	1	2000	MeOH	400	0	$Zn(NO_3)_2$
ZIF-8^{mono}-11000 rpm	No	1	11000	MeOH	400	0	$Zn(NO_3)_2$
ZIF-8^{mono}-dil	No	1	4200	MeOH	800	0	$Zn(NO_3)_2$
ZIF-8^{mono}-conc	No	1	4200	MeOH	200	0	$Zn(NO_3)_2$
ZIF-8^{mono}-am20	No	1	4200	MeOH	380	20	$Zn(NO_3)_2$
ZIF-8^{mono}-am80	No	1	4200	MeOH	400	80	$Zn(NO_3)_2$
ZIF-8^{mono}-NO_3	No	1	11000	MeOH	120	80	$Zn(NO_3)_2$
ZIF-8^{mono}-Cl_2	No	1	11000	MeOH	120	80	$ZnCl_2$
ZIF-8^{mono}-Ac	No	1	11000	MeOH	120	80	$ZnAc_2$
ZIF-8^{mono}-EtOH	No	1	4200	EtOH	400	0	$Zn(NO_3)_2$
ZIF-8^{mono}-IPA	No	1	4200	IPA	400	0	$Zn(NO_3)_2$
ZIF-8^{mono}-Acw[b]	Yes	1	11000	MeOH	120	80	$ZnAc_2$

[a] The metal-linker ratio was maintained at 1:7.9 for all syntheses.
[b] Improved synthesis, discussed at the end of the results section.

Numerous approaches have been proposed to improve the water stability of ZIF-8 [17]. For example, Xia et al. used a post-synthetic functionalisation strategy using heptalfluorobutyric anhydride to produce a fluorinated ZIF-8 with enhanced superhydrophobicity and acid resistance [18]. Nicola et al. incorporated Mg^{2+} during the synthesis to create a mixed-metal ZIF-8 analogue with up to 20% of the metal sites occupied by the alkaline earth metal, which demonstrated enhanced water stability under acidic conditions [19]. Finally, a water-stable $Mn_{0.5}Cd_{0.5}S$@ZIF-8 catalyst was synthesised via dual post-synthesis ligand and cation exchange treatments and demonstrating promising performance for hydrogen production [20].

Despite the remarkable progress made to improve the water stability of ZIF-8, most research has focused on micro-/nano-sized ZIF-8 particles, overlooking the synthesis of sol-gel-based monoliths [21–24]. These sol-gel-based monoliths are mm to cm size polycrystalline materials composed of densely packed primary nanocrystals. They are particularly appealing for industrial applications since they offer an interesting combination of simple preparation and practicality, while also providing a solution to the post-synthesis challenges of MOFs [21,23,25]. ZIF-8 was the first MOF to be synthesised in monolithic form, reported more than a decade ago [21]. Since then a few studies have modified the synthesis procedure, for example by adding modulators to enhance hydrophobicity or by partially replacing the organic solvent with water [22,23]. However, the impact of key synthesis parameters on the properties of ZIF-8 monoliths, particularly their water stability, remains unexplored.

A common mistake in assessing the water stability of MOFs powders and monoliths is relying on analysing the material post-immersion using techniques like PXRD, FTIR, SEM and N^2 gas adsorption [17,24,26,27]. These analytical techniques are not sufficiently sensitive to detect the dissolution of the MOF's external layer. Alternative techniques for accurately assessing MOFs stability in aqueous media include methods that quantify dissolution or degradation products, such liquid chromatography (LC), mass spectrometry (MS) and UV-Vis spectroscopy, among others [17,26].

Over the past two years, we have employed UV-Vis spectroscopy and inductively coupled plasma optical emission spectroscopy (ICP-OES) to investigate the limitations of ZIF-8 monoliths for dye adsorption in aqueous media. In our first publication, we demonstrated that dye adsorption is confined to the external surface of the adsorbent, which is considerably reduced in monoliths compared to their powder counterparts [24]. Additionally, after the adsorption test, the outer layer of the monoliths peeled off upon drying, a degradation phenomenon not observed in powder forms. In a separate publication, we further report the influence of solution parameters on both dye adsorption and monolith degradation. We also proposed a mechanism in which dye adsorption is facilitated by degradation of the monolith, exposing new adsorption sites. After 6 h of contact time, desorption of the dye occurs as dissolved linkers and metal ions create a new phase that precipitates on the monolith surface. This newly formed layer displaces the adsorbed dye and, upon drying, peels off [28]. However, some questions remain unanswered: Given that the synthesis method influences the properties of the materials, and the synthesis procedure for ZIF-8 monoliths differs from that of powder forms, how do synthesis parameters affect the water stability of the monoliths? Furthermore, if the water stability of the monoliths is improved, how does this influence their dye adsorption performance?

In this study, we systematically varied several synthesis parameters from our previously reported procedure [24] to study their impact on water stability of the resulting ZIF-8 monoliths. Parameters that improved at least two of the desired properties – water stability, monolith size, N_2 adsorption, or phase purity – were used to synthesise an optimised monolith. The water stability of this new monolith was tested in Mili-Q water. Finally, the water stability during rhodamine B (RhB) adsorption for four days was assessed for the improved monolith and compared with our previous findings.

2. Experimental section

2.1. Materials

Zinc nitrate hexahydrate (99%, $Zn(NO_3)_2{\cdot}6H_2O$), zinc chloride (98%, $ZnCl_2$), zinc acetate dihydrate (99%, $Zn(CH_3COO)_2{\cdot}2H_2O$) 2-methylimidazole (98%, $C_4H_6N_2$), methanol (99.9%, CH_4O), aqueous ammonia (28-30%, NH_4OH), ethanol (99.9%, C_2H_6O) and isopropanol (99.5%, C_3H_8O), were purchased from Sigma Aldrich and used without further purification.

2.2. Synthesis

The reference ZIF-8 monolith (ZIF-8^{mono}) was synthesised at room temperature following the procedure reported in our previous work [24]: 10 mmol of zinc nitrate hexahydrate and 79 mmol of 2-methylimidazol were each dissolved in 200 mL of methanol separately. The two solutions were mixed and ultrasonicated during 15 min at room temperature. The resulting white mixture was aged for 1 h, then centrifugated at 4200 rpm for 30 min. The collected solid was air-dried overnight to yield monoliths of varying sizes.

The original protocol was then systematically adjusted while keeping the metal-linker ratio constant, in order to evaluate the effect of various

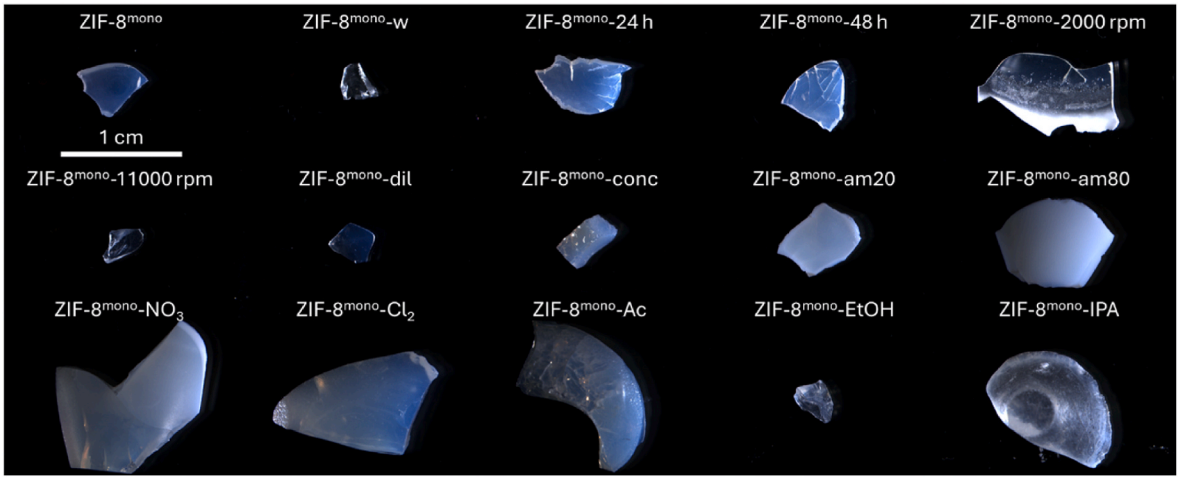

Fig. 1. Optical images in reflection mode of all synthesised monoliths.

synthesis parameters. For example, to assess the influence of the remaining unreacted precursors, monolithic samples were prepared following the original recipe but washing the collected solid three times with methanol prior to air-drying. The detailed washing procedure is provided in supplementary information (ESI).

Seven parameters were varied: the washing procedure, aging time, centrifugal speed, precursor concentration, solvent type, ammonia concentration and metal salt. Table 1 shows a summary of the modified parameters to obtain all the monoliths of this work. The full detailed procedure is presented in ESI (section S.I.1).

Most syntheses were designed to modify only one parameter at a time. This was not feasible for experiments using $ZnCl_2$ (ZIF-8^{mono}-Cl_2) and $ZnAc_2$ (ZIF-8^{mono}-Ac) as precursor materials, as multiple parameters had to be adjusted. To isolate the effect of the salt, the same modified recipe was applied using $Zn(NO_3)_2$ to form ZIF-8^{mono}-NO_3. The modified recipe will be referred to as 'recipe 2' throughout the text.

2.3. Characterisation

PXRD. X-ray diffraction (XRD) measurements were performed on a PXRD, KIBS Bruker D8 Discover XRD, using Cu Kα radiation (λ = 1.5406 Å). The tube operating mode was set at U = 40 kV and I = 40 mA. Two ranges of 2θ diffraction angles were used: 10° - 80° and 5° - 40°, both with a step size of 0.01° and an exposure time of 1 s.

FTIR. A Bruker Invenio-R spectrometer equipped with a diamond attenuated total reflection (ATR) accessory was used for the analysis. All spectra were collected at room temperature within the wavenumber range between 400 and 4000 cm^{-1}, with each spectrum representing the accumulation of 256 scans at a spectral resolution of 4 cm^{-1}.

SEM. Scanning electron microscopy images were acquired using a Zeiss FIB-SEM Crossbeam 550 operated at an accelerating voltage of 5 kV and a beam current of 100 pA.

TGA. The thermogravimetric analysis was performed in a PerkinElmer EGA 4000. Samples in alumina crucibles were heated from 30 to 800 °C at a rate of 10 °C min^{-1} rate. The experiments were conducted under nitrogen atmosphere (99.999%) with a constant flow rate of 40 mL min^{-1}.

N_2 adsorption-desorption measurements. The N_2 isotherm and the pore textural properties (surface area and pore volume) of ZIF-8 monoliths were determined using a Micromeritics TriStar II Plus instrument. Prior to analysis, all samples were activated at 80°C for 20 h using a Micromeritics SmartVacPrep instrument equipped with a hybrid turbo vacuum pump. BET surface areas were calculated using isotherm points between 0.0005 and 0.1 P/P_0. The pore size distribution was determined by non-local density functional theory (NLDFT) using a Tarazona model on cylindrical pores.

2.4. Evaluation of water stability

Water stability experiments were carried out in triplicate at room temperature. For each monolith, 100 mg of the as-synthesised material was added to 50 mL of Mili-Q water and stirred for 24 h. Since monolith degradation releases 2mIm linkers, the process was monitored by UV-Vis spectroscopy by tracking the increase in the absorption band at 205 nm. To that end, aliquots of approximately 250 μL were withdrawn from the flask hourly up to 9 h and at 24 h. The UV-Vis spectra were recorded in the 200 – 300 nm range using a Shimadzu UV-2600i with a medium scan rate (approx. 3 nm s^{-1}) and a step size of 0.5 nm. As an example, the UV-Vis spectra obtained during the first repetition using ZIF-8^{mono} are shown in Fig. S1.

The percentage of degradation was estimated using UV-Vis spectroscopy by determining the amount of 2mIm linkers dissolved in the water in which the monoliths were immersed. To determine the concentration of linkers in water from the UV-Vis spectra, a calibration curve of 2mIm in water with concentrations ranging from 0.1 to 4 mM was obtained (Fig. S2). The estimated concentrations were subsequently used to calculate the percentage of degradation [24]:

$$Degradation\ (\%) = \frac{C_{2mIm} V_s}{2 \cdot W_{ZIF-8} M_{ZIF-8}} 100 = \frac{n_{mIm}}{n_{ZIF-8}} 100 \qquad \text{eq. 2}$$

where C_{2mIm} is the molar concentration of 2mIm in water (mmol/L), V_s is the volume of the water (L), $W_{ZIF\text{-}8}$ is the monolith mass (mg), $M_{ZIF\text{-}8}$ is the molecular mass of ZIF-8 (mg/mmol), n is the number of moles of 2mIm/ZIF-8.

Following the immersion of monoliths in water, the metal concentration in water was determined using Inductive Couple Plasma Optical Emission Spectroscopy (ICP-OES). A 2 mL sample solution was digested with 3 mL of inverse aqua regia ($HCl:HNO_3$ = 1:3) in a microwave digestion system at 250°C. After digestion, the solution was diluted to a final volume of 10 mL and subsequently analysed.

2.5. Adsorption experiments

RhB adsorption experiments followed the same procedure described in our previous work. A total of 100 mg of the prepared adsorbent was added to 50 mL of an RhB solution (10 mg L^{-1}). The solution with the adsorbent was stirred in the dark for 96 h. For the UV-Vis analysis, 250 μL aliquots were withdrawn at defined time intervals: hourly from 1 to 9 h, and at 24, 48, 72 and 96 h. The spectra were recorded in the 200-800 nm range using a medium scan rate (approx. 3 nm s^{-1}) and a step size of 0.5 nm. During the analysis, wavelengths of 205 and 554 nm were tracked for 2mIm and RhB, respectively.

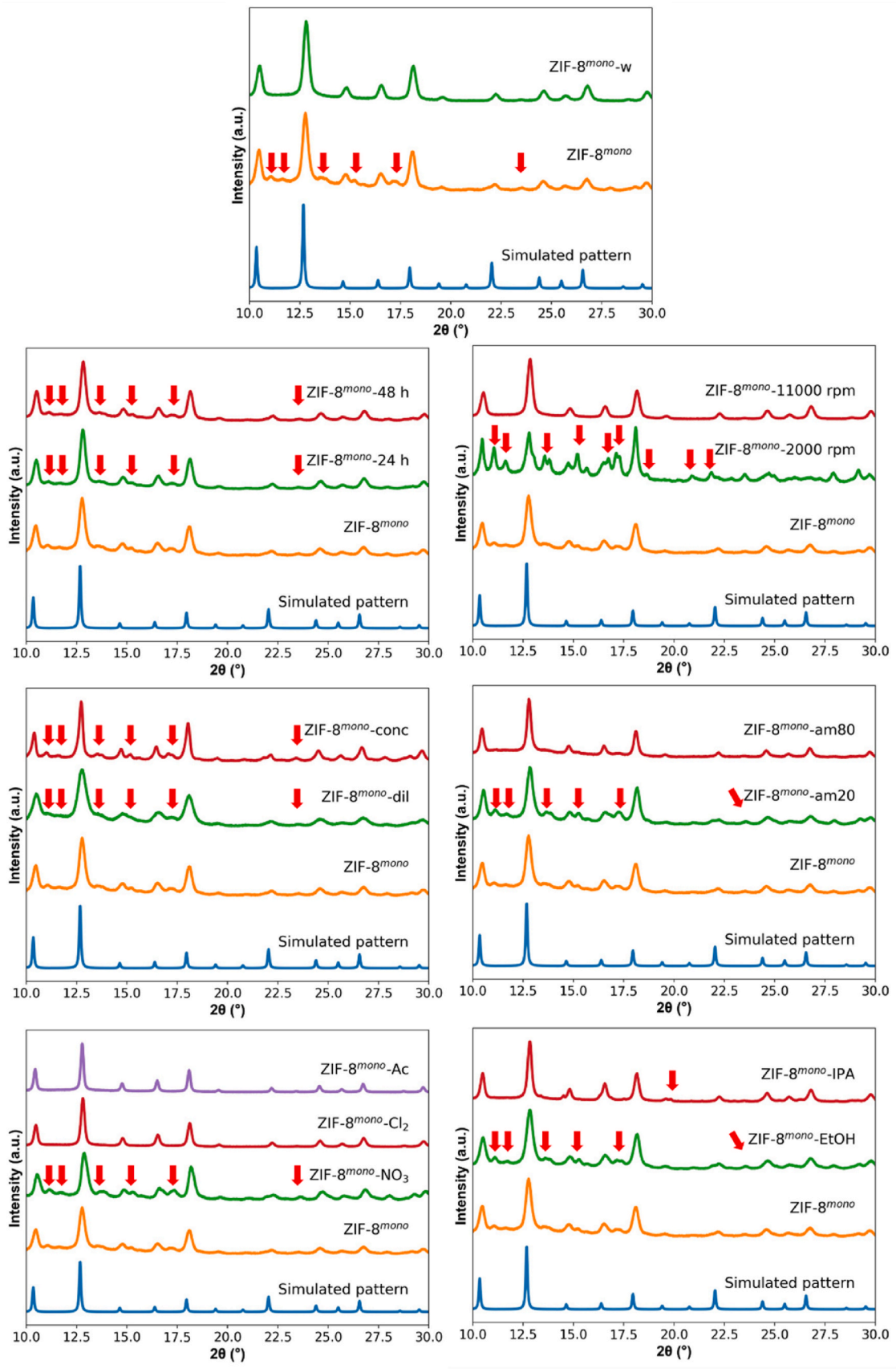

Fig. 2. PXRD pattern of monoliths with modified synthesis compared to the simulated ZIF-8 pattern (blue) and the original synthesis (yellow) over the 2θ of 10 – 30°. The red arrows highlight peaks corresponding to spurious phases. (For interpretation of the references to colour in this figure legend, the reader is referred to the Web version of this article.)

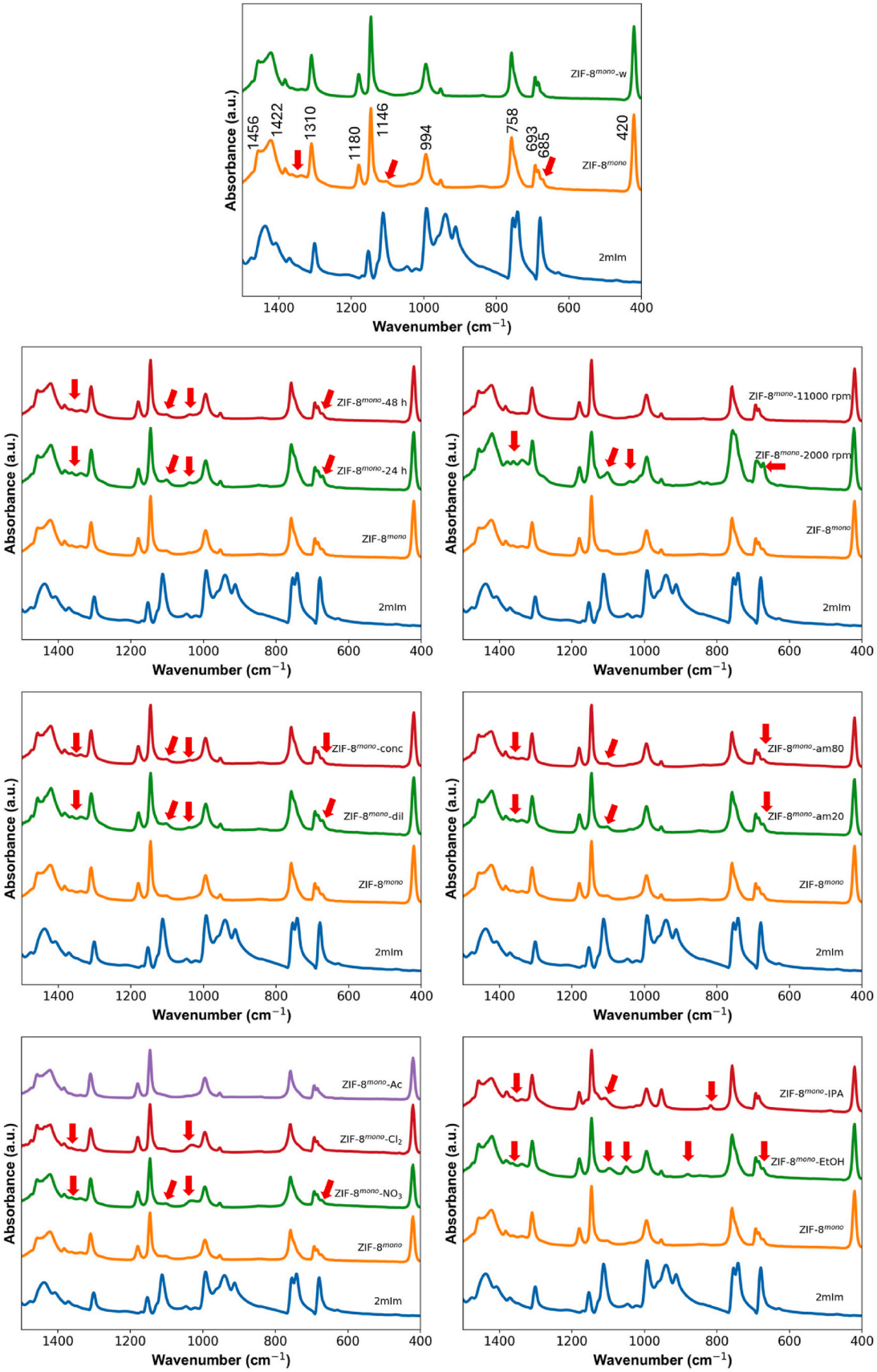

Fig. 3. FTIR spectra of monoliths with modified synthesis compared to spectra of the 2-methylimidazole (blue) and the original synthesis (yellow) in the 400-1500 cm^{-1} range. The red arrows highlight band not corresponding to ZIF-8. (For interpretation of the references to colour in this figure legend, the reader is referred to the Web version of this article.)

Table 2
Peak positions and assigned bands of synthesised monoliths.

Peak(s) cm^{-1}	Assigned band
3136	Stretching mode of C-H_{ring}
1584	-CNH in-plane bending mode of dangling linker due to missing Zn^{2+} ions (defects)
1422 and 1456	C-H_{methyl} bending
1310	Rocking mode of C-H_{ring}
1180	Bending modes from C-H_{ring} with respect to the ring and breathing of the ring
1146	Scissoring and rocking motions of C-H_{ring}
994	Combination of C-H_{methyl} bending and in-plane C-H_{ring} rocking
420	Bending mode between the -CH_3 group and the imidazolate ring
685, 693 and 758[a]	Ring out-of-the-plane bending[a]

[a] The assignation of these bands is based on experimental studies [31–33], whereas the remaining band assignments are based on the computational study by Ahmad et al. [30].

3. Results

The morphology, transparency and colour of monoliths was evaluated by optical microscopy in both reflection mode (Fig. 1) and transmission mode (Fig. S3). The original recipe yielded semi-transparent, irregular monoliths of mm-size. Monoliths of centimetre scale were synthesised using either a MeOH:Aqueous ammonia mixture (ZIF-8^{mono}-Am20, ZIF-8^{mono}-Am80, ZIF-8^{mono}-NO_3, ZIF-8^{mono}-Cl_2 and ZIF-8^{mono}-Ac) or IPA (ZIF-8^{mono}-IPA). Using IPA also produced monoliths that adopted the conical shape of the centrifuge tube and had a slightly granulated texture. At low centrifugal forces (2000 rpm), the resulting monoliths were fragile, wide, large, and flat.

The slight opacity of the monolith may arise from unreacted reagents or unwanted phases formed during the drying. This opacity is further accentuated in transmission-mode optical images (Fig. S3). Parameters that reduced monolith opacity include using the washing procedure (ZIF-8^{mono}-w), diluted solutions (ZIF-8^{mono}-dil) and IPA as solvent (ZIF-8^{mono}-IPA). Partial reduction in monolith opacity occurred at both high (ZIF-8^{mono}-11000 rpm) and low (ZIF-8^{mono}-2000 rpm) centrifugal speeds, as well as when the solvent was replaced for EtOH (ZIF-8^{mono}-EtOH). At low centrifugal speed, the obtained monoliths were mostly transparent with a white segregated phase at one corner. High centrifugal speeds or EtOH as solvent produced a mixture of transparent (Fig. 1 and S3) and slightly opaque pieces (Fig. S4). Finally, white monoliths were obtained using a MeOH:Aqueous ammonia mixture (ZIF-8^{mono}-Am20, ZIF-8^{mono}-Am80, ZIF-8^{mono}-NO_3, ZIF-8^{mono}-Cl_2 and ZIF-8^{mono}-Ac) and high concentrations (ZIF-8^{mono}-conc).

All samples were analysed by PXRD to determine the phase purity and crystallinity. The PXRD diffractograms of all ZIF-8 samples in the 10 – 30° range is displayed in Fig. 2, whereas Fig. S5 presents the full pattern over 5 – 40° range. The full-range pattern demonstrates that most of the samples synthesised in the present work exhibit the characteristic peaks reported for ZIF-8, while the reduced range highlights the presence of a phase distinct from ZIF-8. The peaks belonging to the spurious phases are marked by red arrows in Fig. 2. The original synthesis shows the presence of the spurious phase. However, the intensity of the peaks is relatively weak compared with those from the ZIF-8 phase. Synthesis parameters that eliminate the spurious phases include the washing procedure, a centrifugal speed of 11000 rpm, the addition of 80 mL of aqueous ammonia, and the use of zinc chloride and zinc acetate as initial reagents. Conversely, a centrifugal speed of 2000 rpm promotes the formation of the spurious phase.

To identify the spurious phase, the PXRD patterns of monoliths containing peaks not belonging to ZIF-8 were compared with the simulated pattern of ZIF-L (Fig. S6) [29]. The comparison demonstrates that ZIF-L is the dominant phase at low centrifugal speeds (2000 rpm), whereas it is a minor phase under other conditions. The only exception occurs with IPA as the solvent, where the spurious phase is not attributed to ZIF-L.

Fig. 3 presents the FTIR spectra of all monoliths in the 400 – 1500 cm^{-1} range, while the full spectra (4000 – 400 cm^{-1}) is shown in Fig. S7. Due to the complex nature of the framework, a complete assignment of the observed bands is difficult. However, Table 2 summarises the assignment of most bands, based on the computational study by Ahmad et al. [30] This study does not address the bands in the 650 – 800 cm^{-1} region. Therefore, the assignment of these bands was based on experimental studies [31–33]. Fig. 3 indicates that all samples are identical, displaying several bands that correspond to 2-mIm. The assignments in Table 2 cover most of the intense bands observed in the FTIR spectra. The band around 1584 cm^{-1} (Fig. S7) has been associated with defects, particularly dangling linkers resulting from missing metal ions. Other low-intensity bands, indicated by red arrows in Fig. 3, have been attributed to other defects or impurities within the monoliths. Synthesis parameters that reduced the bands indicated by the red arrows include the washing procedure, a centrifugation at 11000 rpm, and the use of zinc acetate as initial reagent. Contrarily, the intensity of these bands increased when a centrifugation speed of 2000 rpm was used, as well as under diluted synthesis conditions or when IPA was used as synthesis solvent.

TGA up to 800°C was performed to assess the thermal stability of prepared monoliths (Fig. 4). Most of the monoliths exhibit two sharp weight losses: the first at approximately 250°C, attributed to residual material trapped within the pores, and the second at around 600°C, corresponding to the thermal degradation of the sample [21,24]. An additional weight loss observed since the beginning of the measurement is attributed to the evaporation of loosely attached solvent/moisture [34]. This behaviour was noted in the following samples: ZIF-8^{mono}-48 h, ZIF-8^{mono}-conc, ZIF-8^{mono}-am80, ZIF-8^{mono}-NO_3, ZIF-8^{mono}-Cl_2 and ZIF-8^{mono}-IPA. In contrast, ZIF-8^{mono}-Ac shows only one sharp weight loss around 600°C, with the trapped residual material being gradually released between 30°C and 600°C. The use of the washing procedure and a centrifugal speed of 11000 rpm noticeably reduces the weight loss from trapped residual reagents within the pores.

The porosity of the prepared samples was analysed using N_2 adsorption at 77 K. Table 3 summarises the main results of this analysis, while Fig. 5 and Fig. S8 illustrates the N_2 adsorption isotherm in semi-logarithmic and linear scales, respectively. Most samples, excluding ZIF-8^{mono}-2000 rpm, demonstrate the typical ZIF-8 structural flexibility and step-wise N_2 adsorption [35–38]. The step in the isotherms is due to the reorientation of imidazolate linkers, as demonstrated by Fairen-Jimenez et al. [35,39] This behaviour suggests that the samples were indeed microporous (porosity diameter < 2 nm). Both ZIF-8^{mono}-am80 and ZIF-8^{mono}-Cl_2 show a sharp rise in N_2 adsorption close to the saturation pressure. This increase is attributed to N_2 condensation within larger pores present in the sample, suggesting the presence of mesopores [21]. The pore size distribution for the synthesised samples (Figs. S9–S23), determined by non-local density functional theory (NLDFT), confirms that ZIF-8^{mono}-am80 and ZIF-8^{mono}-Cl_2 contain both micropores (10.2-16.7 Å) and mesopores (274.4-448.8 Å), whereas the remaining samples exhibit only micropores (10.2-11.7 Å).

The N_2 sorption data demonstrate that the synthesis parameters influence the adsorption properties of the monoliths. The washing procedure led to a substantial increase in the BET surface area to 1404 $m^2\ g^{-1}$ and the N_2 adsorption capacity to 335 $cm^3\ g^{-1}$, compared to 860 $m^2\ g^{-1}$ and 204 $cm^3\ g^{-1}$ for the original ZIF-8^{mono}. This enhancement stems from the removal of residues within the monolith's pores. Other parameters that improved the BET area and N_2 adsorption capacity include centrifugation at 11000 rpm, diluted and concentrated synthesis, replacing 80 mL of methanol with aqueous ammonia, and using zinc chloride as the initial reagent. In contrast, an aging time of 48 h, replacing 20 mL of methanol with aqueous ammonia, or substituting methanol with IPA greatly reduces the BET area and N_2 adsorption capacity compared to the original monolith.

As observed in N_2 isotherms, the ZIF-8^{mono}-2000 rpm sample

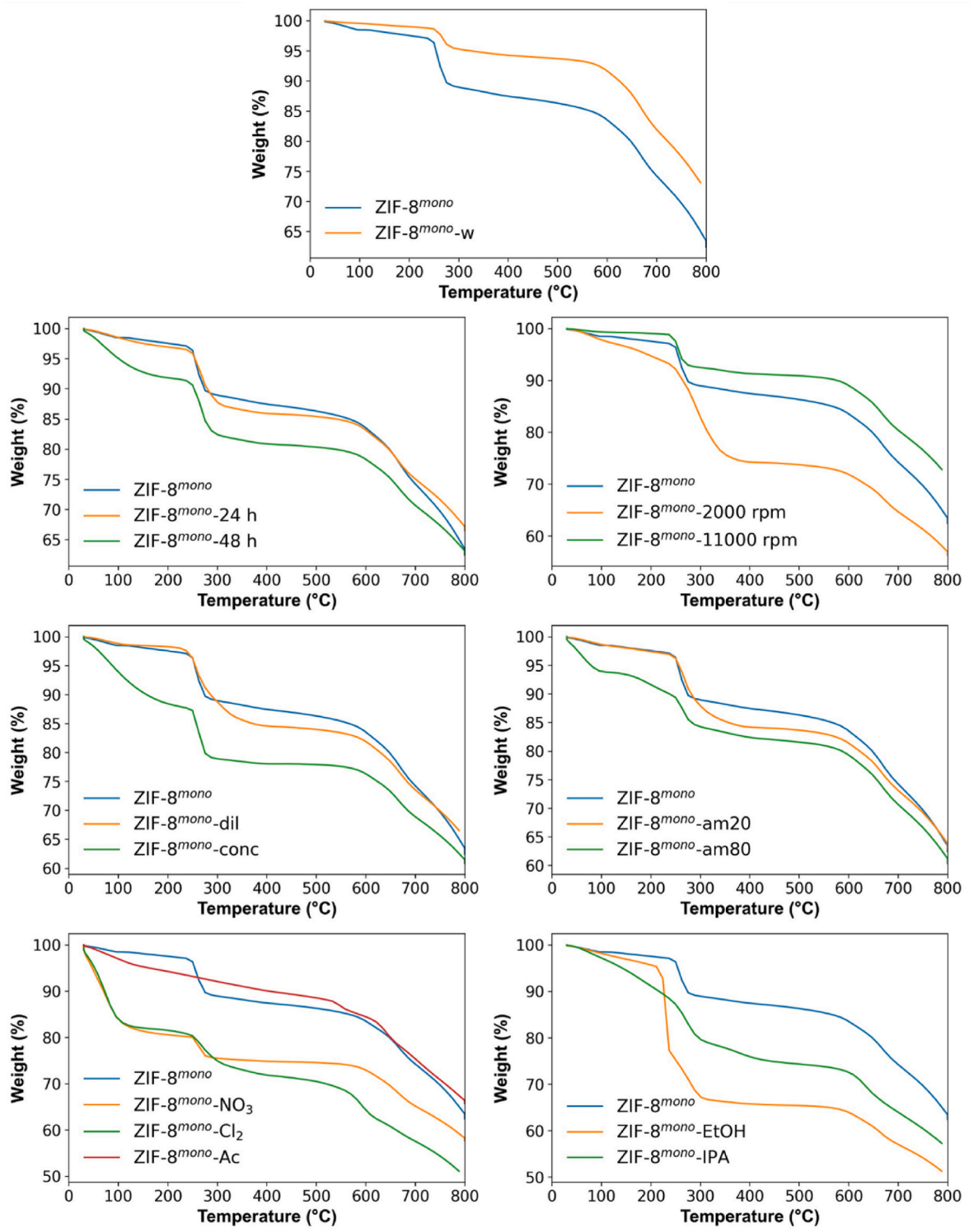

Fig. 4. Thermogravimetric analysis of ZIF-8 monoliths synthesised at different parameters in N_2 atmosphere.

exhibited no porosity. According to the PXRD, the monolith consisted primarily of ZIF-L, whose powder form has much lower BET surface area (67 $m^2\ g^{-1}$) than powder ZIF-8 (1300-1600 $m^2\ g^{-1}$) [40,41]. The even lower BET area of ZIF-8^{mono}-2000 rpm (11 $m^2\ g^{-1}$) is attributed to trapped residual reagents within the pores.

The SEM images of the as-synthesised monoliths offer limited insights, as they typically show flat surfaces. To gain more information from the experiment, SEM images of the precursor particles/gel were collected. Fig. 6 and S24 reveal the morphology of the precursor particles/gel after aging time and before centrifugation. It is noteworthy mention that ZIF-8^{mono}, ZIF-8^{mono}-w, ZIF-8^{mono}-2000 rpm and ZIF-8^{mono}-11000 rpm are synthesised from the same precursor particles. The micrographs show that most of the monoliths are formed of irregular shaped nanoparticles > 100 nm, which merge to form a solid monolith. The aging time allows to obtain smaller nanoparticles, approx. 30 nm for 24 h and approx. 40 nm for 48 h. While diluting the synthesis does not produce a significant change in the precursor nanoparticles, the increase in concentration leads to the formation of approx. 115 nm hollow

Table 3
BET area (S_{BET}), pore diameter obtained from NLDFT (D_{NLDFT}) and total pore volume (W_{total}) of synthesised monoliths.

Material	S_{BET}	D_{NLDFT}	W_{total}
	$m^2\ g^{-1}$	Å	$cm^3\ g^{-1}$
ZIF-8^{mono}	860	11.7	0.311
ZIF-8^{mono} -w	1404	10.9	0.513
ZIF-8^{mono} −24 h	965	10.9	0.360
ZIF-8^{mono} −48 h	634	11.7	0.230
ZIF-8^{mono} −2000 rpm	11	11.7	0.004
ZIF-8^{mono} −11000 rpm	1141	10.9	0.394
ZIF-8^{mono} -dil	1188	10.9	0.447
ZIF-8^{mono} -conc	1023	11.7	0.365
ZIF-8^{mono} -Am20	660	10.9	0.246
ZIF-8^{mono} -Am80	1184	10.2, 16.7, 448.8	0.751
ZIF-8^{mono} -NO_3	752	10.2	0.277
ZIF-8^{mono} -Cl_2	1334	10.2, 16.7, 274.4	0.586
ZIF-8^{mono} -Ac	770	10.9	0.287
ZIF-8^{mono} -EtOH	915	11.7	0.327
ZIF-8^{mono} -IPA	586	10.2	0.225

sphere-like particles. Except when zinc chloride was the initial reagent, adding aqueous ammonia promoted the accelerated blending of ZIF-8 nanoparticles, leading to a rapid consolidation into a solid block during drying of the sample and impairing the visualisation of the precursor particles. The use of EtOH, IPA, or recipe 2 with zinc chloride as the initial reagent yielded ZIF-8 nanoparticles comparable in size and morphology to those synthesised using the original recipe.

3.1. Water stability test

Fig. 7 illustrates the UV-Vis calculated degradation of ZIF-8 monoliths during 24hrs of immersion. Washing slightly improved the water stability of the monoliths. Both washed and unwashed samples show a steady increase in degradation as time progresses, with both approaching a plateau after 24 h, in agreement with prior observations during rhodamine B adsorption in aqueous solutions. While an overlap exists at early times, at longer times the separation is clearer. This is particularly evident at 24 h, where the unwashed material degrades 4% more than washed ZIF-8^{mono}. Similar degradation behaviour was observed for ZIF-8^{mono}-24 h, ZIF-8^{mono}-48 h, ZIF-8^{mono}-conc, and ZIF-8^{mono}-EtOH, with monolith degradation varying slightly (1-3%) compared to the original ZIF-8^{mono}. Notably, water stability was not improved by using centrifugal speed of 11000 rpm. In fact, several parameters, such as a centrifugal speed of 2000 rpm, diluted synthesis, partial substitution of methanol for aqueous ammonia, the use of recipe two with zinc nitrate or zinc chloride as initial reagents, and the replacement of methanol for IPA, were found to reduce the water stability. On the other hand, the use of recipe two with zinc acetate as initial reagent was the only condition that significantly reduced monolith degradation from the beginning of the experiment, lowering water degradation by 4% at 24 h after immersion.

The concentration of Zn^{2+} in water after the immersion of the monoliths was used to further evaluate the degradation of the monoliths. Table 4 demonstrates that the washing procedure and reagent concentration are the two parameters that considerably reduce ion leaching. Monoliths prepared using the original recipe released almost twice as many ions as those made with adjusted regent concentration, and seven times as many as those subjected to the washing procedure. Notably, the monoliths prepared with recipe two and zinc acetate released as many Zn^{2+} ions as those made with zinc nitrate using the original recipe. The parameters that increased Zn^{2+} ion release, and thus monolith degradation, are low centrifuge speed (2000 rpm), the use of IPA as solvent, and recipe two with zinc nitrate as metal salt. These variations in synthesis parameters produced monoliths that released over twice the amount of Zn^{2+} ions compared to those prepared with the original recipe.

The Zn^{2+} ion concentration in the table does not fully represent the total release of ions for all samples. After monolith immersion, the water was filtered to remove all solids. However, precipitates formed in ZIF-8^{mono}-2000 rpm, ZIF-8^{mono}-dil, ZIF-8^{mono}-am20, ZIF-8^{mono}-am80, ZIF-8^{mono}-Cl_2 and ZIF-8^{mono}-IPA after a few days. Interestingly, the precipitate from ZIF-8^{mono}-Cl_2 forms a fine, mobile cluster or network that moves freely in the solution (see supporting video). A second filtration was performed to remove the precipitates before the ICP-OES analysis, which reduced the measured Zn^{2+} ion concentration in these solutions. Even after the filtering out of the precipitate, high Zn^{2+} ion concentrations were detected in water where ZIF-8^{mono}-2000 rpm and ZIF-8^{mono}-IPA were immersed, suggesting very poor stability of these materials. In the case of ZIF-8^{mono}-am80 and ZIF-8^{mono}-Cl_2, most of the released Zn^{2+} ions likely precipitated and were filtered out, resulting in the very low values reported in the table.

PXRD patterns and FTIR spectra of the monoliths after immersion are compared with the as-synthesised monoliths in Fig. S25-S39 and S40-S54, respectively. The results suggest no significant changes in the chemical and structural stability of the monoliths. The PXRD patterns and the FTIR spectra show no appreciable variations in peak intensities, peak broadening, or emergence of new peaks. These observations indicate that PXRD and FTIR are unable to identify the degradation detected by UV-Vis spectroscopy and ICP-OES, in agreement with our previous observations and other literature reports [17,24,26,27].

3.2. Optimal synthesis conditions

The synthesis parameters that improved at least two of the desired properties (water stability, monolith size, N_2 adsorption, or phase purity) were selected as optimal for the preparation of the ZIF-8 monolith. These included the washing procedure, a centrifugal speed of 11000 rpm, concentrated synthesis, partial replacement of methanol for aqueous ammonia and the use of recipe 2 with zinc acetate as the initial reagent. Note that recipe 2 already incorporated a centrifugal speed of 11000 rpm, concentrated synthesis, and partial replacement of methanol for aqueous ammonia, requiring only the addition of the washing procedure to achieve the improved synthesis. Therefore, a new monolith (ZIF-8^{mono}-Acw) was synthesised using zinc acetate, recipe 2 and the washing procedure with MeOH as washing solvent (see ESI).

The synthesised ZIF-8^{mono}-Acw was characterised by optical microscopy, PXRD, FTIR, TGA and N_2 adsorption. The optical images (Fig. 8a and Fig. S55) show that washing removes the unreacted material responsible for the opacity of the original ZIF-8^{mono}-Ac, resulting in transparent, cm-sized monoliths with visible cracking. The PXRD pattern (Fig. 8b and Fig. S26) and FTIR spectrum (Fig. 8c and Fig. S57) confirm the phase purity of the monolith, with no additional peaks observed in either. The TGA profile of ZIF-8^{mono}-Acw (Fig. 8d) exhibits an initial weight loss below 200°C, which is associated with the removal of weakly bonded methanol. A second weight loss, observed around 600°C, corresponds to the thermal decomposition of the framework, consistent with the behaviour observed for the other samples. Finally, the N_2 adsorption analysis (Fig. 8e and Figs. S58–S59, and Table 5) demonstrates that, despite exhibiting a pore size distribution similar to that of ZIF-8^{mono}-Ac, ZIF-8^{mono}-Acw displayed a higher BET surface area, larger total pore volume, and greater N_2 adsorption capacity than both ZIF-8^{mono} and ZIF-8^{mono}-Ac.

The enhanced water stability of ZIF-8^{mono}-Acw was assessed in using PXRD, FTIR, UV-Vis spectroscopy and ICP-OES. PXRD and FTIR shows no difference between the post-immersion and the as-synthesised monolith (Figs. S60–S61). The UV-Vis-calculated degradation (Fig. 9) demonstrated a remarkable improvement in the water stability for ZIF-8^{mono}-Acw since the start of the experiment. After 24 h, ZIF-8^{mono}-Acw exhibited 2.5 and 6.6 % lower degradation compared to ZIF-8^{mono}-Ac and ZIF-$8^{mono,}$ respectively. Additionally, the concentration of Zn^{2+} ions that leached into the solution (Table 6) was reduced under half that of both ZIF-8^{mono}-Ac and ZIF-8^{mono}. These findings suggest that the water

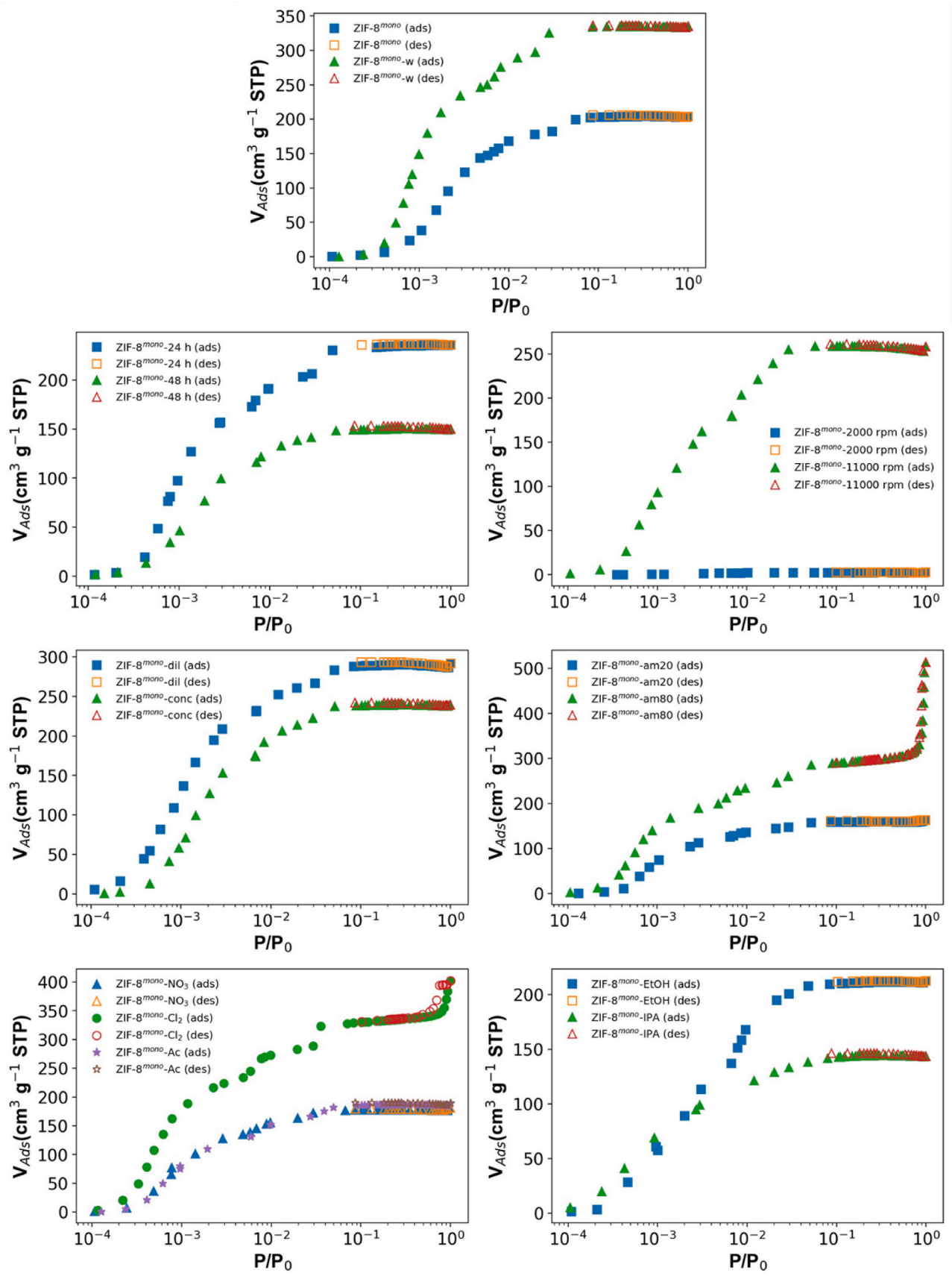

Fig. 5. N_2 adsorption isotherm at 77 K for synthesised monoliths.

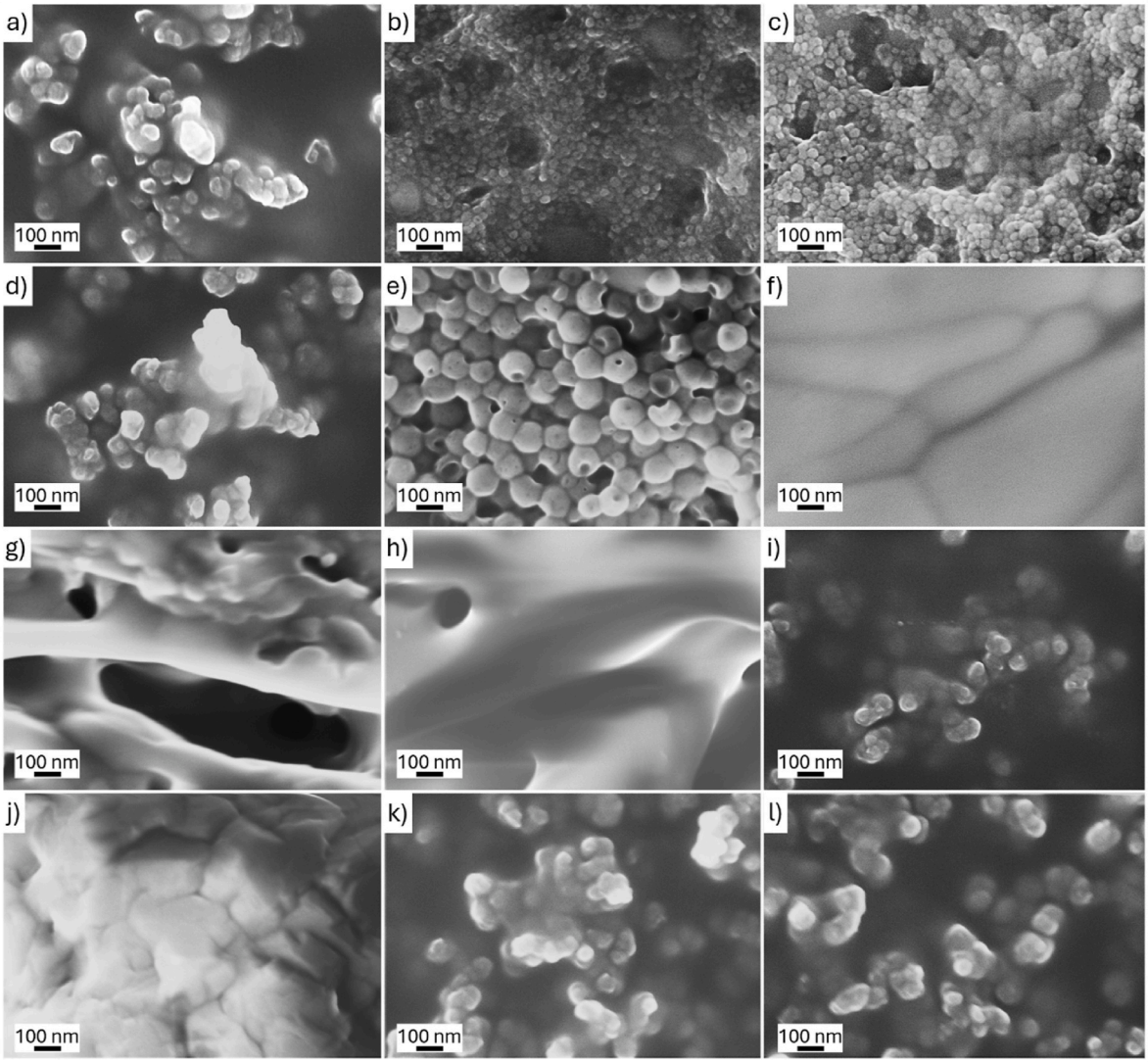

Fig. 6. SEM images of precursor particles/gel of a) ZIF-8^{mono}/ZIF-8^{mono}-w/ZIF-8^{mono}-2000 rpm/ZIF-8^{mono}-11000 rpm, b) ZIF-8^{mono}-24 h, c) ZIF-8^{mono}-48 h, d) ZIF-8^{mono}-dil, e) ZIF-8^{mono}-conc, f) ZIF-8^{mono}-am20, g) ZIF-8^{mono}-am80, h) ZIF-8^{mono}-NO_3, i) ZIF-8^{mono}-Cl_2, j) ZIF-8^{mono}-Ac, k) ZIF-8^{mono}-EtOH, l) ZIF-8^{mono}-IPA.

stability can be improved, though not entirely prevented.

3.3. RhB adsorption test

The water stability and RhB adsorption capacity of ZIF-8^{mono}-Acw were evaluated in a 10 mg L^{-1} RhB solution for four days. As in previous cases, PXRD and FTIR analysis of the monolith post-experiment do not show a change compared with the as-synthesised monolith (Figs. S62–S63). Fig. 10 shows the time-dependent RhB adsorption capacity and UV-Vis-calculated degradation of ZIF-8^{mono}-Acw. As in previous studies, the adsorption was observed in the first hours after immersion, followed by a gradual desorption starting before than 24 h. The negative values observed in the graph are attributed to a small evaporation of the solvent. However, ZIF-8^{mono}-Acw exhibited a lower RhB adsorption capacity (0.30 mg g^{-1}), only 36% of that reported for ZIF-8^{mono} (0.84 mg g^{-1}) [24]. Notably, ZIF-8^{mono}-Acw demonstrated less degradation, with a UV-Vis-calculated degradation of just 3 %, compared to 13 % for ZIF-8^{mono}. Additionally, the ICP-OES analysis revealed that the Zn^{2+} ion concentration in solution with ZIF-8^{mono}-Acw (0.502 mg L^{-1}) was only one-third that of ZIF-8^{mono} (1.4 mg L^{-1}). Despite its superior stability, ZIF-8^{mono}-Acw also exhibited the peeling effect during room-temperature drying, where the outermost layer detaches from the monolith, though this effect was less pronounced than for ZIF-8^{mono} (Fig. S64). These results highlight the critical influence of synthesis parameters on the properties of sol-gel monoliths, with direct implication for their applications.

4. Discussion

The use of different synthesis methods and conditions has led to inconsistent reports on the water stability of micro-/nano-sized ZIF-8 particles [12]. For example, Park et al. demonstrated water stable ZIF-8 via hydrothermal synthesis (DMF, 140 °C, 24 h), with stability in boiling water for up to 7 days, whereas Liu et al. showed that ZIF-8 undergoes hydrolysis under hydrothermal conditions, regardless of particle size (nano- or micro-crystals) or synthesis origin (e.g. water-based) [4,42]. Additionally, Sheng et al. found that using zinc acetate as the precursor material improved the water stability, yet Wang et al. observed the formation of a new phase during the water-stability tests for ZIF-8 synthesised from zinc acetate in basic $NaHCO_3$ and Na_2HPO_4 solutions [16,43]. These conflicting results emphasise that the water-stability of ZIF-8 is highly dependent on synthesis methods and parameters, necessitating systematic studies to tailor its properties.

A similar inconsistency arises with the water stability of sol-gel-based ZIF-8 monoliths. Fairen-Jimenez et al. synthesised ZIF-8 monoliths that remain stable in boiling water for 7 days and demonstrated

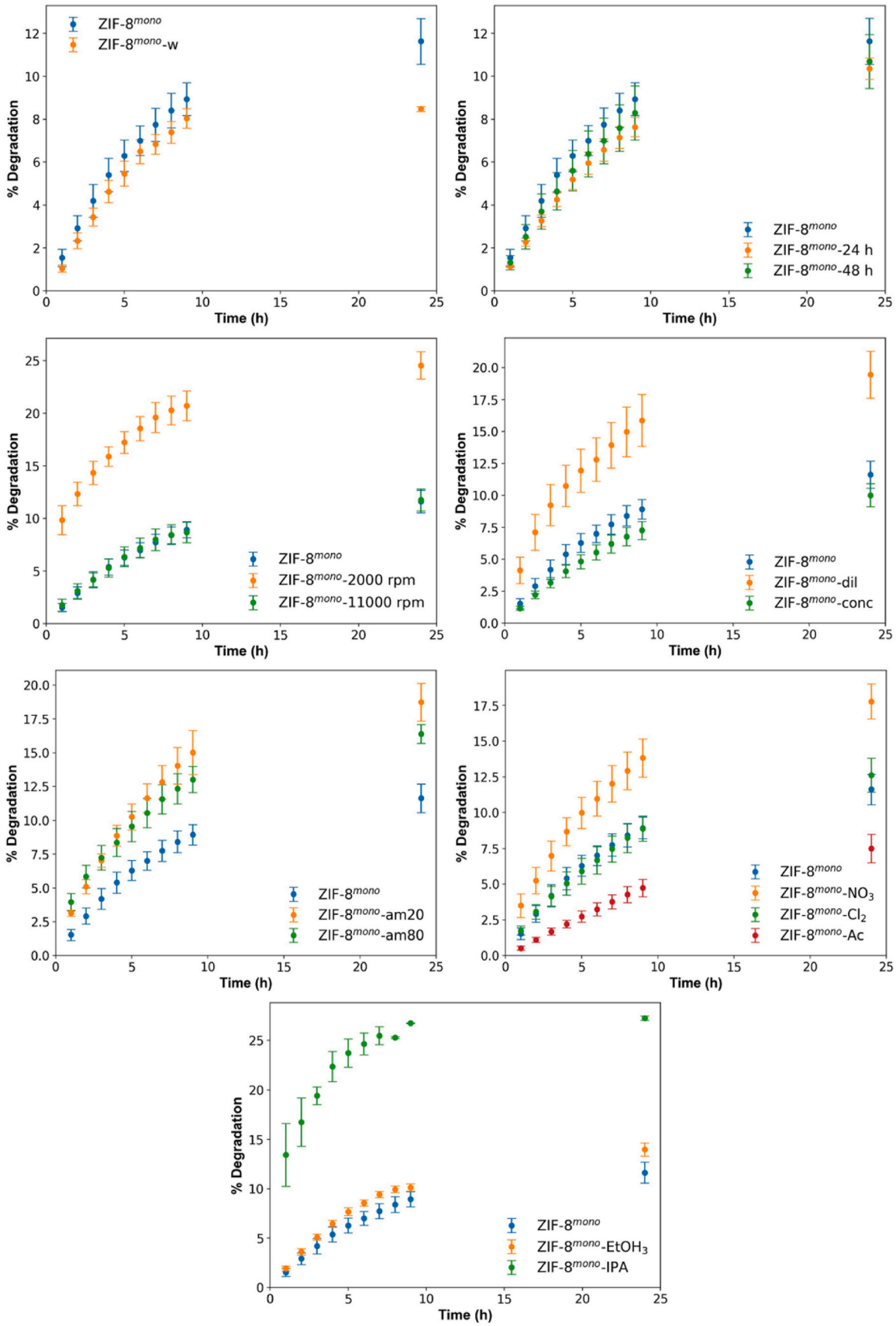

Fig. 7. Time-dependent UV-Vis-calculated degradation of monoliths upon immersion in Mili-Q water.

Table 4
Concentration of Zn^{2+} ions released in water after immersion of monoliths.

Material	C_{Zn} (mg/L)
ZIF-8^{mono}	0.499
ZIF-8^{mono}-w	0.069
ZIF-8^{mono}-24 h	0.367
ZIF-8^{mono}-48 h	0.440
ZIF-8^{mono}-2000 rpm[a]	1.13
ZIF-8^{mono}-11000 rpm	0.582
ZIF-8^{mono}-dil[a]	0.834
ZIF-8^{mono}-conc	0.287
ZIF-8^{mono}-am20[a]	0.614
ZIF-8^{mono}-am80[a]	0.039
ZIF-8^{mono}-NO_3	1.28
ZIF-8^{mono}-Cl_2[a]	< 0.06
ZIF-8^{mono}-Ac	0.468
ZIF-8^{mono}-EtOH	0.717
ZIF-8^{mono}-IPA[a]	1.28

[a] The Zn^{2+} ion content was affected by precipitate formation after the water stability test; this precipitate was filtered out prior ICP-OES analysis.

their applicability for photocatalytic degradation of methylene blue when SnO_2 nanoparticles are encapsulated [21,44]. In contrast, we have reported the instability of sol-gel-based ZIF-8 monoliths during the adsorption of RhB in water: while the monoliths initially exhibited slow RhB uptake, their degradation triggered a gradual desorption within 24 h [24]. These discrepancies emerge from the differences in the synthesis procedure and the methodology used to assess the stability of ZIF-8 monoliths. Fairen-Jimenez et al. employed ethanol as the washing and reaction solvent, with centrifugal speeds exceeding 4000 rpm, whereas we used methanol as the reaction solvent, a centrifugal speed of 4200 rpm, and omitted the washing step due to difficulties forming the monolith afterward. Furthermore, Fairen-Jimenez et al. relied on PXRD and BET to evaluate monolith stability after water test, methods that have shown to be ineffective for assessing water stability [24,26]. In contrast, our water stability test analysed post-experiment solutions using UV-Vis spectroscopy and ICP-OES. To further understand the discrepancy between reports, we conducted the systematic study of this work, clarifying the influence of synthesis parameters on the properties of the monoliths, with a focus on water stability, and using our synthesis procedure as starting point.

The washing procedure is one of the most critical synthesis parameters affecting monolith properties. Unlike micro-/nano-sized particles, monolith synthesis continues after centrifugation, and residual materials post-centrifugation plays a pivotal role. Without washing, the unreacted reagents react with the formed ZIF-8 particles, favouring ZIF-L formation, a phase detected in the PXRD patterns in various monoliths of this work. Additionally, the unreacted reagents opacified the monoliths and reduced both the BET surface area and water stability. While some researchers may find this obvious, some reports cite Tian et al. [45] or Connolley et al. [46] as demonstrating that slow evaporation of the remaining solvent in the presence of unreacted reagents promotes interaction between precursor nano-crystallites by allowing the reaction to continue [23,47,48]. Note that this requires a residual supernatant/washing solvent with a specific metal:linker:solvent ratio, which cannot be guaranteed. However, Tian et al. only proposed this idea without providing experimental evidence, and it was later repeated by Connolley et al. also as a suggestion. Therefore, we recommend researchers to treat this type of suggestion as an invitation for further exploration rather than as evidence.

Another key parameter affecting the water stability of sol-gel-based ZIF-8 monoliths is the choice of metal salt used as the initial reagent. Consistent with the findings of *Sheng* et al., $Zn(CH_3COO)_2$ significantly enhanced the water stability of the monolith [16]. It also prevents the formation of spurious phases, an issue observed with $ZnCl_2$ or $Zn(NO_3)_2$, where the PDXRD patterns and/or FTIR spectra revealed peaks corresponding to phases other than ZIF-8. However, the lack of washing reduced the BET surface area and allowed Zn^{2+} leaching at levels comparable to those observed for monoliths prepared using the original recipe. Additionally, the rate of nucleation of $Zn(CH_3COO)_2$ greatly affects the reaction procedure. Zinc acetate exhibits the lowest nucleation rate among the three salts, following the trend: $Zn(NO_3)_2 \gg ZnCl_2 > Zn(CH_3COO)_2$ [49,50]. While the high nucleation rate of $Zn(NO_3)_2$ produces a large number of nanocrystallites that later form the monolith, the lower nucleation rate of $Zn(CH_3COO)_2$ and $ZnCl_2$ results in few nuclei, which hinders monolith formation under the same synthesis conditions as $Zn(NO_3)_2$. To address this, recipe 2, employing $Zn(CH_3COO)_2$ or $ZnCl_2$, uses higher concentrations of initial solutions and aqueous ammonia. This increases the pH level and the number of deprotonated ligands, promoting nucleus formation and enabling their linking into a monolith structure.

The centrifugal speed has minimal influence on micro-/nano-sized ZIF-8 particles but plays a crucial role in the synthesis and properties of ZIF-8 monoliths. More supernatant is retained in the collected solid when the centrifugal force is low (e.g., 2000 rpm). This includes leftovers of unreacted reagents that favour the synthesis of ZIF-L during the slow drying at room temperature. This ZIF-L monolith has poor water stability and no porosity. To minimise the formation of this unwanted phase and favour the more stable ZIF-8, centrifugal forces of at least 4000 rpm are required. Better results are achieved at higher centrifugal forces (around 11000 rpm) since this reduces the amount of the retained supernatant. This, in turn, reduces the formation of spurious phases, as confirmed by the PXRD and the FTIR spectra of ZIF-8^{mono}-1100 rpm. Even if the washing step is omitted, such strong centrifugal forces reduce the amount of unreacted reagents, favouring the formation of transparent monoliths with slightly higher BET surface areas. They do not, however, provide an improvement in the water stability of the monolith.

According to the IUPAC, aging is defined as the time dependent changes in the chemical or the physical structure and the properties of the gel [51]. It can involve syneresis, coarsening, ripening and phase transformations. In metal-organic gels, aging has been demonstrated to influence the structure and properties of the final material [52,53]. In this work, aging for 24 h homogenises and reduces the size of precursor nanocrystallites. However, extending the aging time to 48 increases the particle size likely due to the Ostwald ripening effect. Unfortunately, this change in particle size did not considerably improve the monolith's properties, such as size, purity, surface area or water stability, possibly due to the slight formation of the ZIF-L, which resulted from the omission of the washing step.

Reactant concentration is a key parameter influencing the characteristics of ZIF-8 particles and monoliths. The results of this work are consistent with those reported by Lai et al., whereby the particle size increases when the amount of MeOH decreases [54]. This was seen in SEM images of precursor crystallites, where ZIF-8^{mono}-conc displayed the biggest particle size. According to Lai et al., this is caused by decrease in the quantity of formed nuclei and a stimulation in the crystal growth at high reactant concentrations. Furthermore, the reactant concentration has an additional effect on the structure of the ZIF-8 monoliths. Low concentrations caused the non-flowing gel, obtained after centrifugation, to retain more supernatant, which led to a greater shrinkage during the drying phase and the formation of thin monolithic pieces. On the other hand, higher reactant concentration produces thicker monoliths, possibly due to a higher density of the non-flowing gel. In both cases the BET surface area improved slightly. However, monoliths produced at low concentrations exhibited poor water stability, most likely as a result of the higher external surface area of the thinner structure.

The ZIF-8 monolith synthesis is extensively affected by the selection of reaction medium. Bustamante et al., and Kim et al., showed that the particle size of the primary crystallites increases with decrease of hydrogen bond donation/acceptance (HBD/HBA) power of the solvent

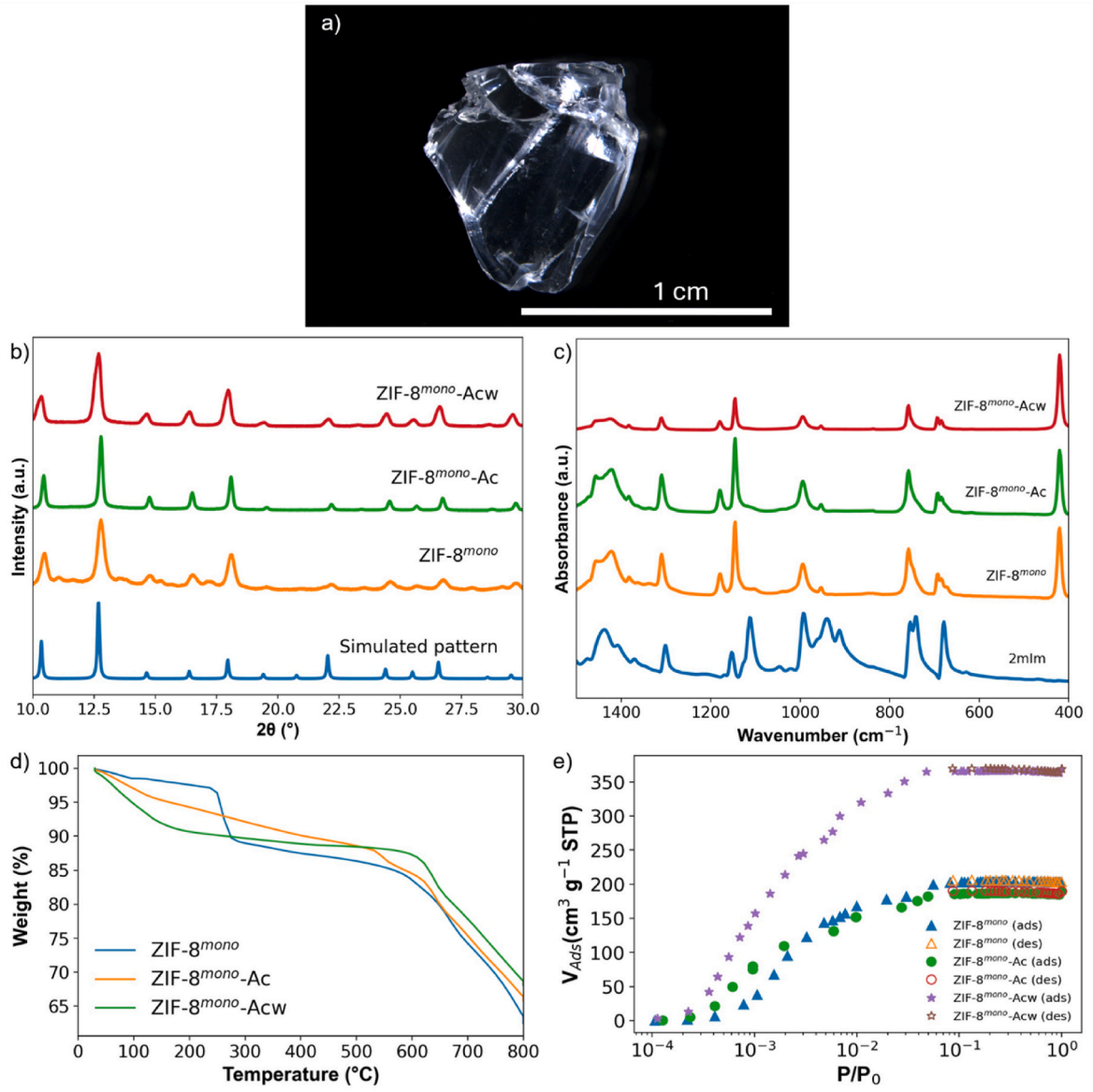

Fig. 8. Characterisation of ZIF-8^{mono}-Acw and its comparison with ZIF-8^{mono} and ZIF-8^{mono}-Ac: a) Optical image of ZIF-8^{mono}-Acw, b) PXRD patterns, c) FTIR spectra, d) TGA profiles and e) N_2 adsorption-desorption isotherm.

Table 5
BET area (S_{BET}), pore diameter obtained from NLDFT (D_{NLDFT}) and total pore volume (W_{total}) of ZIF-8^{mono}, ZIF-8^{mono}-Ac and ZIF-8^{mono}-Acw.

Material	S_{BET}	D_{NLDFT}	W_{total}
	$m^2\ g^{-1}$	Å	$cm^3\ g^{-1}$
ZIF-8^{mono}	860	11.7	0.311
ZIF-8^{mono} -Ac	770	10.9	0.287
ZIF-8^{mono} -Acw	1553	10.9	0.565

[15,55]. In our case, the HBD and HBA followed the trend: MeOH > EtOH > IPA. Therefore, the larger particle size was expected for IPA. However, the SEM images demonstrated no significant change in particle size with variation in the reaction solvent. The difference may come from differences in the synthesis procedure. Although the same molar metal:linker:solvent ratio was used, Bustamante et al., and Kim et al. stirred the mixture for 1 h, while we sonicated for 15 min and aged the mixture for 1 h. Since sonication reduces the particle size due to an increase in the number of nucleation sites [10,56], our synthesis procedure forms primary nanocrystallites of similar size regardless of the reaction solvent. However, the main difference between solvents is observed during the drying step. Since the material was not washed, the drying time varied according to the type of reaction solvent. The drying time for each solvent was overnight, two days and three days for MeOH, EtOH and IPA, respectively (see ESI). As suggested for the FTIR spectra, a slightly higher amount of spurious phases may have formed with ethanol than with methanol due to the slower evaporation of ethanol. These spurious phases led to lower BET surface area as well as thermal and water stability. For IPA, the solvent led to bigger monoliths and less spurious phases, as demonstrated by the optical images, the PXRD pattern and the FTIR spectra. Although this solvent requires more time to evaporate, it has been observed that the formation of the unwanted ZIF-L is less favourable in this solvent [57]. However, the formed monolith has poor water stability properties.

An interesting effect was observed when methanol was partially replaced with aqueous ammonia. This substitution resulted in the formation of remarkably larger monoliths, indicating that the leftover aqueous ammonia within the non-flowing gel affected the syneresis process during the drying step. This is supported by the SEM images,

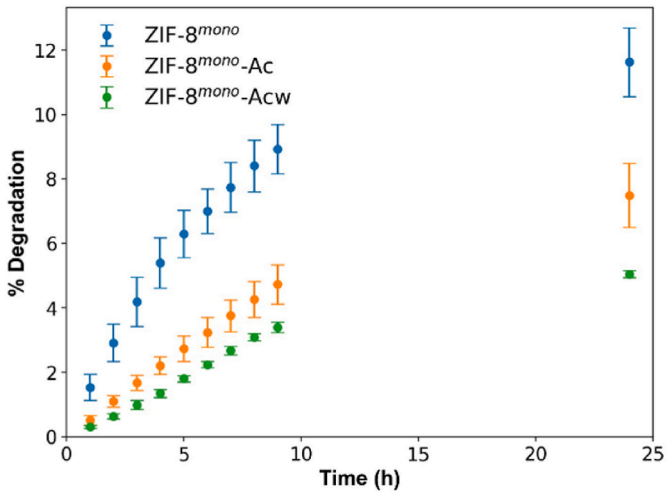

Fig. 9. UV-Vis-calculated degradation of ZIF-8^{mono}, ZIF-8^{mono}-Ac and ZIF-8^{mono}-Acw upon immersion in Mili-Q water.

Table 6
Concentration of Zn^{2+} ions released in water after immersion of ZIF-8^{mono}, ZIF-8^{mono}-Ac and ZIF-8^{mono}-Acw.

Material	C_{Zn} (mg/L)
ZIF-8^{mono}	0.499
ZIF-8^{mono}-Ac	0.468
ZIF-8^{mono}-Acw	0.209

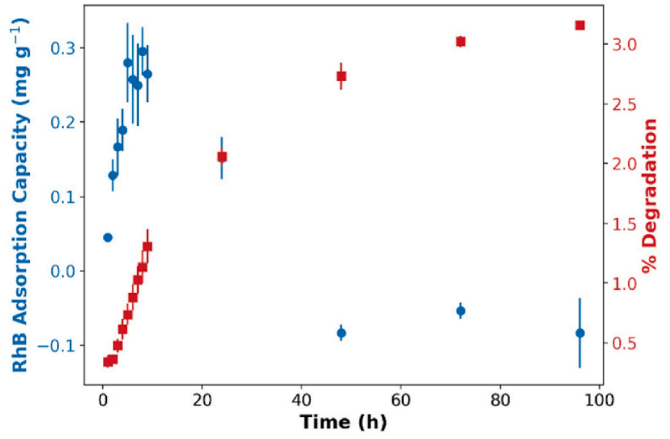

Fig. 10. RhB adsorption capacity and UV-Vis-calculated degradation of ZIF-8^{mono}-Acw.

which suggest that the replacement accelerated the linking between particles during drying. Additionally, the higher pH level also increased deprotonation of the 2mIm linkers, leading to a larger quantity of product compared to the original recipe. This likely reduces the amount of unreacted precursors retained in the non-flowing gel, resulting in higher BET surface area and a reduction in the spurious phases, particularly when 80 mL of methanol were replaced for aqueous ammonia. However, when $Zn(NO_3)_2$ was used as metal salt, the addition of aqueous ammonia reduced the water stability of the resulting monolith. The origin of this effect remains unclear, and further research is needed to explore it.

A ZIF-8 monolith with enhanced water stability was obtained when recipe 2, $Zn(CH_3COO)_2$ and the washing procedure were used. The materials also demonstrated good thermal stability, high BET surface area, and phase purity. Although the monoliths tend to be large, they show several cracks which makes them fragile in some cases. This is attributed to the use of MeOH as washing solvent instead of the reaction mixture MeOH-aqueous ammonia. While aqueous ammonia promotes the formation of bigger monoliths, the washing procedure replaces most of it with MeOH, altering the gel's shrinkage behaviour during densification. This emphasises the importance of the washing solvent.

Despite the enhanced water stability of the later monolith, its RhB adsorption remained poor. This was attributed to the difference in adsorbate's size relative to the adsorbent's pore dimension [24]. The size of the RhB molecule (13.1 × 5.5 × 1.8 Å) far exceeds the window size (3.4 Å) of ZIF-8 [58,59]. Therefore, the dye is adsorbed only on the external surface of the monolith, as stated in our previous work [24]. Additionally, the adsorption occurs as a result of the degradation process. As observed in the previous section, the adsorption only occurs when the degradation shows a linear trend with contact time. On the other hand, desorption is observed when the degradation curve begins to plateau, or slightly earlier. In a recent work, we attributed this behaviour to adsorption happening only at metal sites where linkers that detached due to degradation, while desorption takes place when the concentration of the linkers and metal ions is high enough to form a precipitate that replaces the adsorbed RhB molecules from the monolith's external surface. As the monolith synthesised with the original recipe showed lower stability than the enhanced monolith (ZIF-8^{mono}-Acw), this also exhibited higher RhB adsorption. Note that both monoliths' degradation curves begin to plateau at comparable times but with different linker concentrations. This suggests that the equilibrium conditions were altered as a result of the different characteristics of the enhanced monolith, most likely due to defects.

It is worth noting that this study has limitations that must be acknowledged. First, our study focuses only on seven parameters: washing procedure, aging time, centrifugal speed, precursor concentration, solvent type, ammonia concentration and metal salt. Other critical parameters were omitted, such as metal:linker ratio, reaction temperature, aging temperature, drying conditions, type of washing solvent, among others. We found the use of different washing solvents particularly appealing, since monoliths with distinct properties may be produced using the same synthesis procedure but varying the washing solvent. A second limitation is the omission of the washing step in most of the syntheses. Although this allowed us to demonstrate that, regardless of the conditions, the remaining reagents do not promote the linking between crystallites, and that the presence of unreacted precursors and the formation of ZIF-L compromise the properties of the synthesised monoliths and complicate comparisons.

5. Conclusions

ZIF-8 continues to be employed in water purification applications, even for adsorbing molecules much larger than pore size. However ZIF-8 is not stable in water, and its dye uptake is limited to the external surface area. Here, we demonstrate that even with an improved water stable version, ZIF-8 monoliths still degrade, albeit at a much slower rate. Additionally, we showed that dye uptake depends on degradation, that create new adsorption sites, consistent with our proposed mechanism reported elsewhere. This is not observed in powder forms, likely due to different defects, highlighting the need to further investigate the influence of defects on the water stability, dye adsorption, and photocatalytic degradation of dyes in ZIF-8 monoliths.

More systematic studies are necessary to further improve the synthesis of ZIF-8 monoliths, since not all parameters were tested. Here, washing procedure, aging time, centrifugal speed, precursor concentration, solvent type, ammonia concentration and metal salt were systematically varied to refine a previously reported synthesis protocol. The appropriate washing procedure is one of the most important parameters to enhance phase purity, transparency, BET surface area and water

stability. Another crucial parameter is the metal salt. The water stability mostly improved by using $Zn(CH_3COO)_2$ instead of $Zn(NO_3)_2$ as the initial precursor. However, the low nucleation rate of $Zn(CH_3COO)_2$ required substantial adjustments to the synthesis protocol, including high reactant concentration, centrifugal speeds exceeding 4200 rpm, and partial substitution of methanol with aqueous ammonia (at least 80 mL). Fortunately, our analysis demonstrated that the individual change of these parameters produced desirable effects on two or more of the desired properties of the monolith. Nevertheless, parameters such as the metal:linker ratio, reaction temperature, aging temperature, drying conditions and type of washing solvent must be analysed to further optimise the properties of ZIF-8 monoliths.

This work provides a systematic map of how synthesis parameters influence the textural properties, size, chemical composition, and most importantly the water stability of the ZIF-8 monoliths, allowing researchers to rationally tailor synthesis conditions to improve material performance. Researchers can use this work as a foundation to optimise other properties not investigated here, such as mechanical strength and malleability during drying, which is important for shaping and processing ZIF-8 monoliths. Additionally, we provide an optimised and reproducible synthesis protocol for a more water-stable ZIF-8 monolith that researchers can use for further experiments or as a base to improve the chemical stability of ZIF-8, instead of the previously reported protocols.

We also quantify, for the first time, how varying monolith synthesis parameters affect water stability. This was achieved by analysing the water post-immersion using a combination of UV-Vis spectroscopy and ICP-OES, rather than examining the monolith itself after immersion. This enables us to determine an approximately 7% reduction in degradation for the improved monolith after 24 h of immersion in water. This study supports the growing trend of analysing water post-immersion, since this provides more information than the traditional analysis.

CRediT authorship contribution statement

Jose de Jesus Velazquez-Garcia: Writing – review & editing, Writing – original draft, Supervision, Investigation, Formal analysis, Data curation, Conceptualization. **Susann Frenzke:** Supervision. **Dina Huanaco-Quispe:** Investigation. **Henry Sanchez Cornejo:** Investigation. **Luis de los Santos Valladares:** Investigation. **Crispin H.W. Barnes:** Resources. **Christopher Copeman:** Investigation. **Jatinder Singh:** Investigation. **Stefanie Haugg:** Investigation. **Dirk Eifler:** Investigation. **Simone Techert:** Supervision, Resources, Funding acquisition.

Declaration of competing interest

The authors declare that they have no known competing financial interests or personal relationships that could have appeared to influence the work reported in this paper.

Acknowledgments

The work in Peru was supported by a Collaboration Agreement between the Universidad Nacional Autonoma de Huanta (Peru) and the University of Cambridge (UK), Contract Number G117323. H. S. C. thanks the Peruvian Agency CONCYTEC for financial support through grant No. PE501095272-2025-PROCIENCIA. We are grateful to the Deutsche Forschungsgemeinschaft (DFG, German Research Foundation) for the financial support provided for project C04/SFB 1633 “Proto-coupled electron transfer” and under Germany's Excellence Strategy – EXC 3120/1 –533771286. HG-recruitment, HG-Innovation “FISCOV” and “FISVIR” and the CMWS are also thanked for financial support. Additionally, we are grateful to the BlueMAT for their financial contribution. We acknowledge Prof. Ashlee J. Howarth for providing access to the instrumentation for conducting the N_2 adsorption measurements in this study. We also thank the Zentrale Element-Analytik at the University of Hamburg, Germany, for performing the ICP-OES analysis. We acknowledge the use of the Hamburg-CRR cleanroom facility, jointly operated by UHH, DESY, and MPSD.

Appendix A. Supplementary data

Supplementary data to this article can be found online at https://doi.org/10.1016/j.micromeso.2026.114368.

Data availability

Data will be made available on request.

References

[1] L. Kotvytska, R. Tarasenko, O. Lyutakov, M. Erzina, N. Tomašovičová, O. Vinnik, M. Orendáč, A. Orendáčová, Physical properties of metal–organic zeolitic imidazolate frameworks, APCOM 2778 (2023) 040015, https://doi.org/10.1063/5.0136197.
[2] B. Chen, Z. Yang, Y. Zhu, Y. Xia, Zeolitic imidazolate framework materials: recent progress in synthesis and applications, J. Mater. Chem. A 2 (2014) 16811–16831, https://doi.org/10.1039/C4TA02984D.
[3] Q. Wang, D. Astruc, State of the art and prospects in metal–organic framework (MOF)-based and MOF-derived nanocatalysis, Chem. Rev. 120 (2020) 1438–1511, https://doi.org/10.1021/acs.chemrev.9b00223.
[4] K.S. Park, Z. Ni, A.P. Côté, J.Y. Choi, R. Huang, F.J. Uribe-Romo, H.K. Chae, M. O'Keeffe, O.M. Yaghi, Exceptional chemical and thermal stability of zeolitic imidazolate frameworks, Proc. Natl. Acad. Sci. USA 103 (2006) 10186–10191, https://doi.org/10.1073/pnas.0602439103.
[5] X. Gong, Y. Wang, T. Kuang, ZIF-8-Based membranes for carbon dioxide capture and separation, ACS Sustainable Chem. Eng. 5 (2017) 11204–11214, https://doi.org/10.1021/acssuschemeng.7b03613.
[6] M.P. Suh, H.J. Park, T.K. Prasad, D.-W. Lim, Hydrogen storage in metal–organic frameworks, Chem. Rev. 112 (2012) 782–835, https://doi.org/10.1021/cr200274s.
[7] D. Behera, P. Priyadarshini, K. Parida, ZIF-8 metal–organic frameworks and their hybrid materials: emerging photocatalysts for energy and environmental applications, Dalton Trans. 54 (2025) 2681–2708, https://doi.org/10.1039/D4DT02662D.
[8] R. Ahmad, U.A. Khan, N. Iqbal, T. Noor, Zeolitic imidazolate framework (ZIF)-derived porous carbon materials for supercapacitors: an overview, RSC Adv. 10 (2020) 43733–43750, https://doi.org/10.1039/D0RA08560J.
[9] Q. Wang, Y. Sun, S. Li, P. Zhang, Q. Yao, Synthesis and modification of ZIF-8 and its application in drug delivery and tumor therapy, RSC Adv. 10 (2020) 37600–37620, https://doi.org/10.1039/D0RA07950B.
[10] Y.-R. Lee, M.-S. Jang, H.-Y. Cho, H.-J. Kwon, S. Kim, W.-S. Ahn, ZIF-8: a comparison of synthesis methods, Chem. Eng. J. 271 (2015) 276–280, https://doi.org/10.1016/j.cej.2015.02.094.
[11] K. Yang, M. Ni, C. Xu, L. Wang, L. Han, S. Lv, W. Wu, D. Zheng, Microfluidic one-step synthesis of a metal−organic framework for osteoarthritis therapeutic microRNAs delivery, Front. Bioeng. Biotechnol. 11 (2023) 1239364, https://doi.org/10.3389/fbioe.2023.1239364.
[12] C.-X. Jin, H.-B. Shang, Synthetic methods, properties and controlling roles of synthetic parameters of zeolite imidazole framework-8: a review, J. Solid State Chem. 297 (2021) 122040, https://doi.org/10.1016/j.jssc.2021.122040.
[13] C.S. Cereceda, Y. Du, Effect of synthesis parameters on ZIF-8 morphology: insights from experimental and statistical integrated analysis, Microporous Mesoporous Mater. 390 (2025) 113588, https://doi.org/10.1016/j.micromeso.2025.113588.
[14] Y. Zhang, Y. Jia, M. Li, L. Hou, Influence of the 2-methylimidazole/zinc nitrate hexahydrate molar ratio on the synthesis of zeolitic imidazolate framework-8 crystals at room temperature, Sci. Rep. 8 (2018) 9597, https://doi.org/10.1038/s41598-018-28015-7.
[15] E.L. Bustamante, J.L. Fernández, J.M. Zamaro, Influence of the solvent in the synthesis of zeolitic imidazolate framework-8 (ZIF-8) nanocrystals at room temperature, J. Colloid Interface Sci. 424 (2014) 37–43, https://doi.org/10.1016/j.jcis.2014.03.014.
[16] L. Sheng, F. Yang, C. Wang, J. Yu, L. Zhang, Y. Pan, Comparison of the hydrothermal stability of ZIF-8 nanocrystals and polycrystalline membranes derived from zinc salt variations, Mater. Lett. 197 (2017) 184–187, https://doi.org/10.1016/j.matlet.2017.03.077.
[17] E. Wahid, W.A. El-Mehalmey, A. Naser, M. Amin, B.R. Brooks, A.S. Mayhoub, M. H. Alkordi, Mechanism of hydrolytic instability of ZIF-8 in aqueous and buffered media: implications on drug delivery applications, ACS Omega 11 (2026) 18952–18960, https://doi.org/10.1021/acsomega.5c11300.
[18] X. Xia, J. Liu, Y. Xiao, Y. Yu, Y. Ren, J. Chen, W. Xie, B. Yang, J. Zhang, Z. Yang, W. Hu, H. Yang, Superhydrophobic acid-resistant fluorinated Zif-8 prepared at normal temperature and pressure, Chem. Eng. J. 505 (2025) 159223, https://doi.org/10.1016/j.cej.2025.159223.

[19] N. Di Nicola, E. Spoletti, P. Cezade, A. Lazzarini, M. Lusi, An Mg solid solution affords a less toxic and more stable ZIF-8, ACS Omega 11 (2026) 26629–26634, https://doi.org/10.1021/acsomega.5c13152.

[20] R. Ding, H. Zhu, J. Zhou, H. Luo, K. Xue, L. Yu, Y. Zhang, Highly water-stable and efficient hydrogen-producing heterostructure synthesized from $Mn_{0.5}$ $Cd_{0.5}$ S and a Zeolitic Imidazolate framework ZIF-8 via ligand and cation exchange, ACS Appl. Mater. Interfaces 15 (2023) 36477–36488, https://doi.org/10.1021/acsami.3c08614.

[21] T. Tian, J. Velazquez-Garcia, T.D. Bennett, D. Fairen-Jimenez, Mechanically and chemically robust ZIF-8 monoliths with high volumetric adsorption capacity, J. Mater. Chem. A 3 (2015) 2999–3005, https://doi.org/10.1039/C4TA05116E.

[22] E. Hunter-Sellars, P.A. Saenz-Cavazos, A.R. Houghton, S.R. McIntyre, I.P. Parkin, D.R. Williams, Sol–gel synthesis of high-density zeolitic imidazolate framework monoliths via ligand assisted methods: exceptional porosity, hydrophobicity, and applications in vapor adsorption, Adv. Funct. Mater. 31 (2021) 2008357, https://doi.org/10.1002/adfm.202008357.

[23] A. Pathak, L.A. Alghamdi, J. Fernández-Catalá, M. Tricarico, D. Cazorla-Amorós, J. Tan, Á. Berenguer-Murcia, G. Mehlana, A.E.H. Wheatley, Understanding metal–organic framework densification: solvent effects and the growth of colloidal primary nanoparticles in monolithic ZIF-8, Small 21 (2025) 2500510, https://doi.org/10.1002/smll.202500510.

[24] J. de Jesus Velazquez-Garcia, S. Frenzke, L. de los S. Valladares, C.H.W. Barnes, C. Copeman, J. Singh, S. Kulkarni, T.F. Keller, H.S. Cornejo, D. Huanaco-Quispe, M. Anwary, R. Elorche, L.M. Asprilla-Herrera, W. Łukaszczyk, N. Eroglu, D. Eifler, S. Techert, Size matters: limitations of the ZIF-8 monolith and its Ni-, Co- and Cu-doped variants for the adsorption of rhodamine B, Mater. Adv. 6 (2025) 7800–7811, https://doi.org/10.1039/D5MA00797F.

[25] B.M. Connolly, D.G. Madden, A.E.H. Wheatley, D. Fairen-Jimenez, Shaping the future of fuel: monolithic metal–organic frameworks for high-density gas storage, J. Am. Chem. Soc. 142 (2020) 8541–8549, https://doi.org/10.1021/jacs.0c00270.

[26] M. Taheri, T.G. Enge, T. Tsuzuki, Water stability of cobalt doped ZIF-8: a quantitative study using optical analyses, Mater. Today Chem. 16 (2020) 100231, https://doi.org/10.1016/j.mtchem.2019.100231.

[27] M.T. Nord, A.S. Plaman, L.N. Zakharov, O.K. Farha, M. Nyman, Acid stability of M^{IV} (M = Zr, Hf, Ce, th) UiO-66 MOFs from a solution perspective, ACS Appl. Mater. Interfaces 17 (2025) 21357–21370, https://doi.org/10.1021/acsami.4c21721.

[28] J.D.J. Velazquez-Garcia, S. Frenzke, S. Abdulrahman, H. Abdulla, R. Elorche, M. Anwary, C. Bintas, E.N. Pujol, C. Copeman, H. Sanchez Cornejo, D. Huanaco-Quispe, L. De Los Santos Valladares, C.H.W. Barnes, D. Eifler, S. Techert, Not Only the Size Matters: Effect of Solution Parameters on Dye Adsorption by ZIF-8 Monoliths, 2026 submitted for publication.

[29] R. Chen, J. Yao, Q. Gu, S. Smeets, C. Baerlocher, H. Gu, D. Zhu, W. Morris, O. M. Yaghi, H. Wang, A two-dimensional zeolitic imidazolate framework with a cushion-shaped cavity for CO2 adsorption, Chem. Commun. 49 (2013) 9500, https://doi.org/10.1039/c3cc44342f.

[30] M. Ahmad, R. Patel, D.T. Lee, P. Corkery, A. Kraetz, Prerna, S.A. Tenney, D. Nykypanchuk, X. Tong, J.I. Siepmann, M. Tsapatsis, J.A. Boscoboinik, ZIF-8 vibrational spectra: peak assignments and defect signals, ACS Appl. Mater. Interfaces 16 (2024) 27887–27897, https://doi.org/10.1021/acsami.4c02396.

[31] Y. Hu, H. Kazemian, S. Rohani, Y. Huang, Y. Song, In situ high pressure study of ZIF-8 by FTIR spectroscopy, Chem. Commun. 47 (2011) 12694, https://doi.org/10.1039/c1cc15525c.

[32] Y. Zhang, Y. Jia, L. Hou, Synthesis of zeolitic imidazolate framework-8 on polyester fiber for PM2.5 removal, RSC Adv. 8 (2018) 31471–31477, https://doi.org/10.1039/C8RA06414H.

[33] V. Nozari, C. Calahoo, J.M. Tuffnell, D.A. Keen, T.D. Bennett, L. Wondraczek, Ionic liquid facilitated melting of the metal-organic framework ZIF-8, Nat. Commun. 12 (2021) 5703, https://doi.org/10.1038/s41467-021-25970-0.

[34] F.S. Butt, A. Lewis, F. Dingwall, N.A. Mazlan, N. Radacsi, X. Fan, X. Chen, Y. Yang, S. Yang, Y. Huang, ZIF-8 with exceptional thermal stability: role of organic cosolvents in phase control and structure stabilization, Mater. Today Chem. 34 (2023) 101804, https://doi.org/10.1016/j.mtchem.2023.101804.

[35] D. Fairen-Jimenez, S.A. Moggach, M.T. Wharmby, P.A. Wright, S. Parsons, T. Düren, Opening the gate: framework flexibility in ZIF-8 explored by experiments and simulations, J. Am. Chem. Soc. 133 (2011) 8900–8902, https://doi.org/10.1021/ja202154j.

[36] C.O. Ania, E. García-Pérez, M. Haro, J.J. Gutiérrez-Sevillano, T. Valdés-Solís, J. B. Parra, S. Calero, Understanding gas-induced structural deformation of ZIF-8, J. Phys. Chem. Lett. 3 (2012) 1159–1164, https://doi.org/10.1021/jz300292y.

[37] L. Zhang, Z. Hu, J. Jiang, Sorption-induced structural transition of zeolitic imidazolate Framework-8: a hybrid molecular simulation study, J. Am. Chem. Soc. 135 (2013) 3722–3728, https://doi.org/10.1021/ja401129h.

[38] C. Zhang, J.A. Gee, D.S. Sholl, R.P. Lively, Crystal-size-dependent structural transitions in nanoporous crystals: adsorption-induced transitions in ZIF-8, J. Phys. Chem. C 118 (2014) 20727–20733, https://doi.org/10.1021/jp5081466.

[39] D. Fairen-Jimenez, R. Galvelis, A. Torrisi, A.D. Gellan, M.T. Wharmby, P.A. Wright, C. Mellot-Draznieks, T. Düren, Flexibility and swing effect on the adsorption of energy-related gases on ZIF-8: combined experimental and simulation study, Dalton Trans. 41 (2012) 10752, https://doi.org/10.1039/c2dt30774j.

[40] A.M. Nasir, N.A.H. Md Nordin, P.S. Goh, A.F. Ismail, Application of two-dimensional leaf-shaped zeolitic imidazolate framework (2D ZIF-L) as arsenite adsorbent: kinetic, isotherm and mechanism, J. Mol. Liq. 250 (2018) 269–277, https://doi.org/10.1016/j.molliq.2017.12.005.

[41] Q. Song, S.K. Nataraj, M.V. Roussenova, J.C. Tan, D.J. Hughes, W. Li, P. Bourgoin, M.A. Alam, A.K. Cheetham, S.A. Al-Muhtaseb, E. Sivaniah, Zeolitic imidazolate framework (ZIF-8) based polymer nanocomposite membranes for gas separation, Energy Environ. Sci. 5 (2012) 8359, https://doi.org/10.1039/c2ee21996d.

[42] X. Liu, Y. Li, Y. Ban, Y. Peng, H. Jin, H. Bux, L. Xu, J. Caro, W. Yang, Improvement of hydrothermal stability of zeolitic imidazolate frameworks, Chem. Commun. 49 (2013) 9140, https://doi.org/10.1039/c3cc45308a.

[43] H. Wang, M. Jian, Z. Qi, Y. Li, R. Liu, J. Qu, X. Zhang, Specific anion effects on the stability of zeolitic imidazolate framework-8 in aqueous solution, Microporous Mesoporous Mater. 259 (2018) 171–177, https://doi.org/10.1016/j.micromeso.2017.10.011.

[44] J.P. Mehta, T. Tian, Z. Zeng, G. Divitini, B.M. Connolly, P.A. Midgley, J. Tan, D. Fairen-Jimenez, A.E.H. Wheatley, Sol–gel synthesis of robust metal–organic frameworks for nanoparticle encapsulation, Adv. Funct. Mater. 28 (2018) 1705588, https://doi.org/10.1002/adfm.201705588.

[45] T. Tian, Z. Zeng, D. Vulpe, M.E. Casco, G. Divitini, P.A. Midgley, J. Silvestre-Albero, J.-C. Tan, P.Z. Moghadam, D. Fairen-Jimenez, A sol–gel monolithic metal–organic framework with enhanced methane uptake, Nat. Mater. 17 (2018) 174–179, https://doi.org/10.1038/nmat5050.

[46] B.M. Connolly, M. Aragones-Anglada, J. Gandara-Loe, N.A. Danaf, D.C. Lamb, J. P. Mehta, D. Vulpe, S. Wuttke, J. Silvestre-Albero, P.Z. Moghadam, A.E. H. Wheatley, D. Fairen-Jimenez, Tuning porosity in macroscopic monolithic metal-organic frameworks for exceptional natural gas storage, Nat. Commun. 10 (2019) 2345, https://doi.org/10.1038/s41467-019-10185-1.

[47] J. Hou, A.F. Sapnik, T.D. Bennett, Metal–organic framework gels and monoliths, Chem. Sci. 11 (2020) 310–323, https://doi.org/10.1039/C9SC04961D.

[48] W. Zhang, X. Wu, X. Peng, Y. Tian, H. Yuan, Solution processable metal–organic frameworks: synthesis strategy and applications, Adv. Mater. 37 (2025) 2412708, https://doi.org/10.1002/adma.202412708.

[49] G. Ramu, M. Lee, H.-K. Jeong, Effects of zinc salts on the microstructure and performance of zeolitic-imidazolate framework ZIF-8 membranes for propylene/propane separation, Microporous Mesoporous Mater. 259 (2018) 155–162, https://doi.org/10.1016/j.micromeso.2017.10.010.

[50] A. Schejn, L. Balan, V. Falk, L. Aranda, G. Medjahdi, R. Schneider, Controlling ZIF-8 nano- and microcrystal formation and reactivity through zinc salt variations, CrystEngComm 16 (2014) 4493–4500, https://doi.org/10.1039/C3CE42485E.

[51] J.V. Alemán, A.V. Chadwick, J. He, M. Hess, K. Horie, R.G. Jones, P. Kratochvíl, I. Meisel, I. Mita, G. Moad, S. Penczek, R.F.T. Stepto, Definitions of terms relating to the structure and processing of sols, gels, networks, and inorganic-organic hybrid materials (IUPAC recommendations 2007), Pure Appl. Chem. 79 (2007) 1801–1829, https://doi.org/10.1351/pac200779101801.

[52] Z. Wang, C. Villa Santos, A. Legrand, F. Haase, Y. Hara, K. Kanamori, T. Aoyama, K. Urayama, C.M. Doherty, G.J. Smales, B.R. Pauw, Y.J. Colón, S. Furukawa, Multiscale structural control of linked metal–organic polyhedra gel by aging-induced linkage-reorganization, Chem. Sci. 12 (2021) 12556–12563, https://doi.org/10.1039/D1SC02883A.

[53] A.M. Shaiful Bahari, S.Z. Othman, M.F. Mohamad Fadli, M.Z.A. Zulkifli, S. A. Biyamin, M.A. Islam, Z. Aspanut, N. Amin, H. Misran, Facile synthesis of Zr-based metal-organic gel (Zr-MOG) using "green" sol-gel approach, Surf. Interfaces 27 (2021) 101469, https://doi.org/10.1016/j.surfin.2021.101469.

[54] L.S. Lai, Y.F. Yeong, N. Che Ani, K.K. Lau, M.S. Azmi, Effect of the solvent molar ratios on the synthesis of zeolitic imidazolate framework 8 (ZIF-8) and its performance in CO2 adsorption, Appl. Mech. Mater. 625 (2014) 69–72, https://doi.org/10.4028/www.scientific.net/AMM.625.69.

[55] Y.J. Kim, M.-Z. Kim, S.F. Alam, A.U. Rehman, A. Devipriyanka, P. Sharma, H. R. Lee, C.-H. Cho, Polarity-dependent particle size of zeolitic imidazolate framework synthesized in various solvents, Mater. Chem. Phys. 259 (2021) 124021, https://doi.org/10.1016/j.matchemphys.2020.124021.

[56] S. Nalesso, G. Varlet, M.J. Bussemaker, R.P. Sear, M. Hodnett, R. Monteagudo-Oliván, V. Sebastián, J. Coronas, J. Lee, Sonocrystallisation of ZIF-8 in water with high excess of ligand: effects of frequency, power and sonication time, Ultrason. Sonochem. 76 (2021) 105616, https://doi.org/10.1016/j.ultsonch.2021.105616.

[57] A. Lewis, F.S. Butt, X. Wei, N.A. Mazlan, Z. Chen, Y. Yang, S. Yang, N. Radacsi, X. Chen, Y. Huang, Crystallization and phase selection of zeolitic imidazolate frameworks in aqueous cosolvent systems: the role and impacts of organic solvents, Results Eng. 17 (2023) 100751, https://doi.org/10.1016/j.rineng.2022.100751.

[58] B. Luan Tran, H.-Y. Chin, B.K. Chang, A.S.T. Chiang, Dye adsorption in ZIF-8: the importance of external surface area, Microporous Mesoporous Mater. 277 (2019) 149–153, https://doi.org/10.1016/j.micromeso.2018.10.027.

[59] X. Fan, W. Wang, W. Li, J. Zhou, B. Wang, J. Zheng, X. Li, Highly porous ZIF-8 nanocrystals prepared by a surfactant mediated method in aqueous solution with enhanced adsorption kinetics, ACS Appl. Mater. Interfaces 6 (2014) 14994–14999, https://doi.org/10.1021/am5028346.